Spatiotemporal transcriptomic analysis during cold ischemic injury to the murine kidney reveals compartment-specific changes

Srujan Singh[1,2], Shishir Kumar Patel[3], Ryo Matsuura[3], Dee Velazquez[1,2], Zhaoli Sun[4], Sanjeev Noel[3], Hamid Rabb[3]*, Jean Fan[1,2]*

[1]Center for Computational Biology, Whiting School of Engineering, Johns Hopkins University, Baltimore, Maryland, USA

[2]Department of Biomedical Engineering, Johns Hopkins University, Baltimore, Maryland, USA

[3]Department of Medicine, Johns Hopkins University, Baltimore, Maryland, USA

[4]Department of Surgery, Johns Hopkins University, Baltimore, Maryland, USA

Correspondence should be addressed to:

Hamid Rabb (hrabb1@jhmi.edu)

Jean Fan (jeanfan@jhu.edu)

Key words: spatial transcriptomics, cold ischemia, warm ischemia, kidney transplant

Abstract:

Kidney transplantation is the gold standard treatment strategy for end-stage renal disease. Deceased donor kidneys usually undergo cold storage until kidney transplantation, leading to cold ischemia injury that may contribute to poor graft outcomes. However, the molecular characterization of potential mechanisms of cold ischemia injury remains incomplete. To bridge this knowledge gap, we leveraged spatial transcriptomics technology to perform full transcriptome characterization of cold ischemia injury (0-48 hours) using a murine model. We developed a computational workflow to identify spatiotemporal transcriptomic changes that accompany the injury pathophysiology in a compartment-specific manner. We identified potential metabolic reprogramming preferentially within the kidney inner medulla displaying strong oxidative phosphorylation signature in an ischemic environment. We found commonalities between the spatiotemporal transcriptomic presentation of cold ischemia and warm ischemia–reperfusion injury, including an induction of an anti-viral like immune response throughout the renal tissue. Altogether, these systems-level biological insights enabled by our full transcriptome temporal characterization unveil a molecular basis for how cold ischemia injury may negatively affect kidney outcomes. Moreover, our spatial analyses highlight pathological developments deep within the renal tissue, suggesting potential opportunities for new insights beyond biopsy-focused superficial tissue examinations. We also developed an interactive online browser at https://jef.works/vitessce-cold-ischemia/ to facilitate exploration of our results by the broader scientific and clinical community.

Introduction:

Kidney transplantation remains the gold standard treatment strategy for end-stage renal disease, relying on viable allografts from either living or deceased donors. Although live donor kidneys usually have better short and long-term graft outcomes, their limited availability has contributed to a major push to expand the deceased donor pool (*1*). A key challenge with deceased donor kidneys is the cold ischemia time (CIT) —the period during which the kidneys are preserved in cold storage after procurement and before transplantation (*2–4*). In this period, kidneys are flushed with cryopreserving solution and kept on ice to minimize cellular injury and preserve the organ viability during the transit between transplantation centers. The kidneys experience cold ischemia injury (*5*) during this phase, which can lead to delayed graft function and poor graft outcomes (*6*).

The pathophysiology of cold ischemia induced renal injury is incompletely understood. While prior studies (*7–9*) have sought to characterize processes that are believed to accompany cold ischemia and lead to cellular injury, they usually do not recapitulate the complex structure of kidney tissue. Moreover, these studies primarily investigate only a few targeted cold ischemia related pathological processes and their associated biomarkers, potentially overlooking other clinically relevant pathological developments. Additionally, findings from several large cohort, multi-variate retrospective studies (*6*, *10–13*) lack consensus on a standard clinically acceptable CIT for kidney allografts. Collectively, this highlights the opportunity for a more thorough molecular characterization of cold ischemia injury of the entire kidney to elucidate the underlying biological processes that may contribute to poor prognosis with increasing CIT.

High-throughput sequencing data-driven approaches can surveil the genome-wide molecular landscape during disease pathogenesis. In particular, advances in spatial transcriptomics (ST) technologies (*14–16*) now enable full transcriptome spatially resolved profiling of gene expression patterns. Such a data-driven approach can facilitate the generation of hypotheses towards the identification of potential biomarkers of prolonged cold ischemia injury and therapeutic targets.

We therefore leveraged 10x Visium ST technology to perform full transcriptome profiling of murine kidneys subject to varying durations of cold ischemia to characterize spatiotemporal molecular changes across typical durations of cold ischemia in a deceased donor renal transplant setting (Fig 1A). Our integrative spatiotemporal computational analyses delineated trends that facilitated the identification of differential spatiotemporal molecular dynamics in a compartment-specific manner, especially pertaining to aberrant metabolic reprogramming, to shed light on how prolonged cold ischemia may contribute to adverse transplant outcomes. An interactive browser with our data and results is available to facilitate exploration at https://jef.works/vitessce-cold-ischemia/

.

Results

1. Computational workflow identifies shared spatial compartment across multiple murine kidney spatial transcriptomics datasets.

To establish a quantitative molecular understanding of cold ischemia across the entire kidney, we applied 10x Visium to perform full transcriptome spatial transcriptomic (resolution: 55 μm pixels/spots) profiling of cold ischemia kidney injury in a murine model. The model introduced 0, 12, 24 and 48 hours of cold ischemia injury that represent typical durations of cold ischemia in a deceased-donor renal transplant setting (Fig. 1A, S1A-D). Quality control filtering resulted in 19454 unique gene species detected across 12530 pixels belonging to the cold ischemia kidney injury tissue specimens (4.18 $\pm$ 0.29 transcripts/spot and 2.6 $\pm$ 0.96 spots/gene ($\log_{10}$ scale)) (Fig. S1E-L). To facilitate comparative analysis across the cold ischemia kidney specimens as well as with kidney specimens from previously published studies (*17*, *18*)(especially, ischemia-reperfusion injury as a model for acute kidney injury (AKI)), we sought to computationally integrate all 17 ST datasets (44816 pixels) to identify transcriptionally similar tissue compartments via graph-based clustering (Fig. 1B). However, such unified clustering was driven by batch effects as well as unique biological processes resulting in condition and sample-specific clusters, thereby hindering the identification of shared features. We therefore performed batch correction using Harmony (17) (Fig. 1C) and re-clustered to identify shared compartments across all datasets (Fig. 1D). Due to lack of single cell resolution and concerns for variations in cell-type proportions confounding small clusters, we opted for coarser clustering. Ultimately, this computational workflow led to identification of distinct compartments which we labeled as cortex, outer medulla (O.Medulla), inner medulla (I.Medulla) based on their relative anatomical location within all the kidney tissue specimens (Fig. 1E, Fig. S1M,N). Review of the corresponding H&E images by an expert renal pathologist validated our labels, confirming congruence between the transcriptional and histological assessments. Remaining tissue which was not part of the previous three compartments was labeled as other, likely corresponding to the transition from

medulla to pelvis based on pathologist's evaluation, and was not used for any analyses henceforth. We were then able to perform differential expression analysis across compartments of all ST datasets (Fig. S2) to identify marker genes of the different compartments, which were found to be consistent with known annotations of associated functional units. For instance, markers for functional units like *Slc14a2* for descending thin limb of Loop of Henle (LOH) and *Slc5a3* for thick descending limb of LOH (*20*) were identified as one of the top gene markers for inner medulla compartment. Similarly, proximal tubule S3 segment marker *Slc22a7* (*21*) was identified as one of the top gene markers for outer medulla while pan-proximal tubule marker *Slc34a1* and proximal convoluted tubule marker *Slc5a2* were associated with the cortex (18) (Fig. S3). This observation was consistent across all datasets. As such, our computational workflow identified spatially distinct compartments, thereby enabling us to further analyze transcriptomic temporal dynamics in the different compartments of kidney tissue.

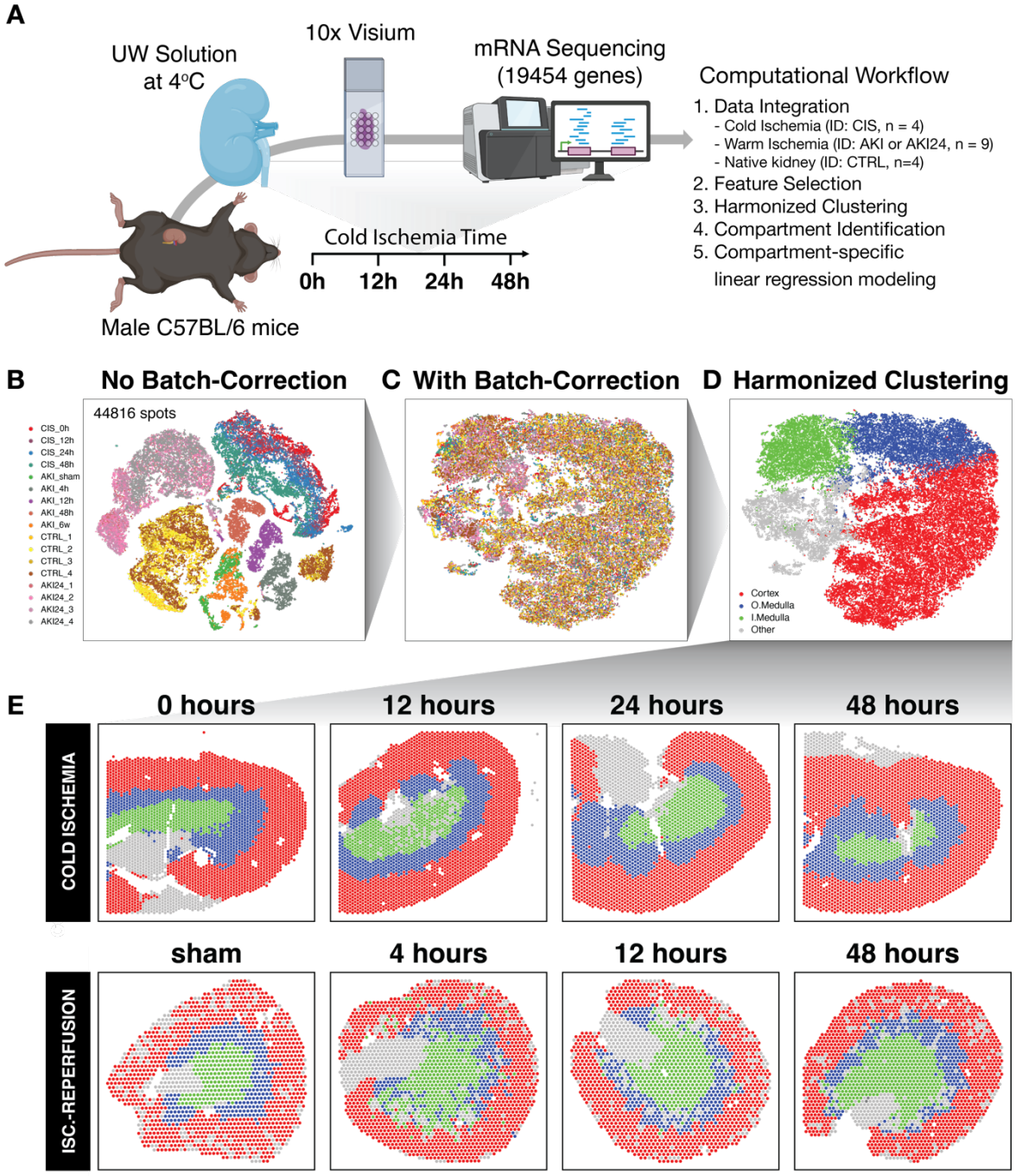

Figure 1. Computational workflow for analysis of multiple murine kidney spatial transcriptomics datasets. (A) Spatial transcriptomics datasets were generated from murine kidneys subjected to cold ischemia injury of various durations: 0, 12, 24 and 48 hours. Thereafter, the datasets were integrated with

previously published ST datasets and subjected to computational analysis. **(B)** tSNE plot demonstrating sample-specific effects within the integrated ST datasets. **(C)** Harmonized tSNE plot leading to a shared embedding across all datasets. **(D)** Clustering facilitated identification of shared transcriptionally distinct compartments across all the datasets, namely cortex, outer medulla (O.Medulla), inner medulla (I.Medulla) and other. **(E)** Spatial plots visualizing the anatomic location of the different transcriptionally-defined compartments within the renal tissue specimens belonging to different experimental groups like cold ischemia injury and ischemia-reperfusion injury. Created with BioRender.com

2. Compartment-specific analysis characterizes spatially confined gene expression dynamics in cold ischemia kidney injury

To characterize the temporal transcriptional dynamics associated with cold ischemia injury, we leveraged linear regression modeling to identify genes with expression patterns that significantly change with duration of cold ischemia injury (i.e., CIT). Briefly, after compartment identification within the kidney samples, we applied linear regression to each compartment separately. Such linear regression modeling identified many genes that decreased gradually in expression magnitude with longer CIT i.e., exhibited a downward temporal trend (number of genes in inner medulla: 2413 (12.4%), outer medulla: 2227 (11.44%) and cortex: 1591 (8.17%))(Table S1). Surprisingly, given lack of blood flow, many other genes gradually increased in expression magnitude with longer cold ischemia time i.e., exhibited an upward temporal trend (inner medulla: 922 (4.7%), outer medulla: 1344 (6.91%) and cortex: 1683 (8.65%))(TableS2). Comparing across compartments, we found genes exhibiting temporal trends either in a compartment-agnostic or compartment-specific manner. For compartment-agnostic trends, 436 (2.24%) genes exhibited an upward temporal trend across all compartments whereas 471 (2.42%) exhibited a downward temporal trend across all compartments (Table S3). For instance, *Fth1* (Fig. 2A), *Igfbp7,* and *Umod* were upregulated over time across all compartments whereas *Kap* (Fig. S4A)*, Gpx3,* and *Acsm2* were

downregulated over time across all compartments. In comparison, there were comparatively more genes that exhibited a compartment-specific temporal trend (upward trend: inner medulla: 275 (1.41%), outer medulla: 394 (2.02%), cortex: 702 (3.61%)(Table S4); downward trend: inner medulla: 1391 (7.15%), outer medulla: 966 (4.97%), cortex: 579 (2.98%) (Table S5)). For example, *Ranbp3l* was uniquely upregulated over time in the inner medulla (Fig. 2B), whereas *Mep1a* was uniquely upregulated in the outer medulla (Fig. 2C), and *Slc34a1* in the cortex (Fig. 2D). In contrast, *Egf* was uniquely downregulated over time in the inner medulla, whereas *Fxyd2* was uniquely downregulated in the outer medulla, and *Aqp1* in the cortex (Fig. S4B-D). Within each compartment, we observed a great variation in the magnitude of gene expression changes (i.e., linear regression slopes) with most genes demonstrating subtle changes (smaller slopes i.e., normalized scores<0.5 (Fig. 2E)) with increasing CIT while a certain number of genes changed remarkably (larger slopes) such as *Fth1, Umod*, and *Kap*. (Fig. 2E, F-H, Table S1,2). To investigate whether these trends covary between compartments, we compared the regression slopes of genes in the different compartments. Pearson correlation analysis suggested that the cortex and outer medulla (Pearson correlation coefficient, PCC= 0.94, $p<0.05$, $R^2= 0.88$) (Fig. 2F) are more similar to each other in terms of temporal gene expression changes as compared to the inner medulla (cortex vs inner medulla: PCC= 0.63, $p<0.05$, $R^2= 0.4$) (Fig. 2G); outer medulla vs inner medulla: PCC= 0.68, $p<0.05$, $R^2= 0.46$) (Fig. 2H)). As such, our compartment-specific temporal analysis identified compartment-agnostic as well as compartment-specific gene expression trends.

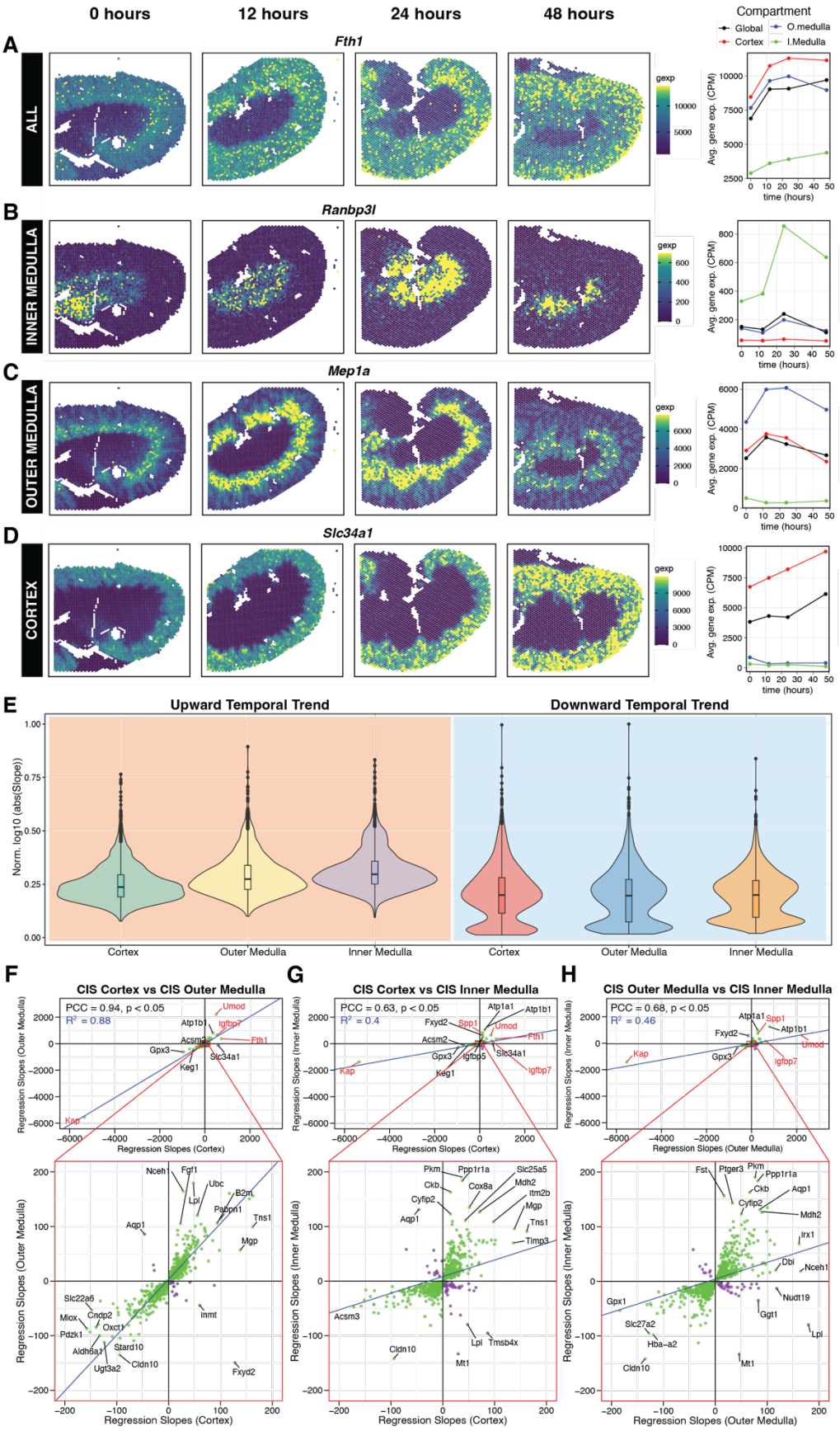
0 hours
12 hours
24 hours
48 hours
Compartment
Global
Cortex
O.medulla
I.Medulla
A
Fth1
ALL
B
Ranbp3l
INNER MEDULLA
C
Mep1a
OUTER MEDULLA
D
Slc34a1
CORTEX
gexp
Avg. gene exp. (CPM)
time (hours)
E
Upward Temporal Trend
Downward Temporal Trend
Norm. log10 (abs(Slope))
Cortex
Outer Medulla
Inner Medulla
F
CIS Cortex vs CIS Outer Medulla
PCC = 0.94, p < 0.05
R² = 0.88
G
CIS Cortex vs CIS Inner Medulla
PCC = 0.63, p < 0.05
R² = 0.4
H
CIS Outer Medulla vs CIS Inner Medulla
PCC = 0.68, p < 0.05
R² = 0.46
Regression Slopes (Cortex)
Regression Slopes (Outer Medulla)
Regression Slopes (Inner Medulla)

Figure 2. Compartment-specific temporal transcriptional dynamics in cold ischemic kidneys. (A) Spatial gene expression plots and corresponding line plots demonstrating spatiotemporal dynamics of representative genes that demonstrated an upward temporal trend during the cold ischemic phase (0-48 hours). For instance, **(A)** *Fth1* was upregulated in all the compartments whereas **(B)** *Ranbp3l,* **(C)** *Mep1a* and **(D)** *Slc34a1* were uniquely upregulated in the inner medulla, outer medulla and cortex compartments of cold ischemic injury renal tissue respectively. **(E)** Violin plots highlight the skewed distribution of magnitude of transcriptional changes (linear regression slopes) within the different compartments of CIS renal tissue. Scatterplots depicting the correlation analysis of the temporal transcriptional dynamics between the different compartments: **(F)** cortex vs outer medulla, **(G)** cortex vs inner medulla and **(H)** outer medulla vs inner medulla of the CIS kidney tissue. Genes exhibiting covarying (green) or divergent (purple) temporal trend within these compartments can be visualized along with their Pearson correlation coefficients (PCC) and linear regression slopes (blue line). Genes which exhibited strong temporal changes like *Fth1, Spp1, Umod, Igfbp7, Kap* within these compartments have been highlighted red.

3. Pathway characterization of identified spatiotemporal trends suggest compartment-specific metabolic reprogramming

To better understand the molecular pathways associated with genes that demonstrated significant time dependent expression with increasing CIT, we performed gene set enrichment analysis on the temporally upregulated and temporally downregulated genes with longer CIT obtained through our previous linear regression analysis ranked by slope in a spatial compartment specific manner (Methods). We identified significantly enriched molecular pathways and evaluated whether they exhibited covarying or divergent trends across different compartments based on their normalized enrichment scores (NES) (Fig. 3A-C, Table S6, S7). Within the renal inner medulla, we observed significant positive enrichment (NES>0) of energy

metabolism pathways amongst several enriched biological pathways (Fig. 3A), suggesting that genes within these pathways were being temporally upregulated in this compartment during cold ischemia injury. For instance, oxidative phosphorylation (OXPHOS) pathway (ID: mmu00190) thermogenesis (ID: mmu04714), and citrate cycle (TCA cycle)(ID: mmu00020) were positively enriched primarily in the inner medulla. In contrast, these pathways demonstrated a weak positive or negative enrichment within the outer medulla and cortex (Fig. 3E-G), suggesting that genes within these pathways were not being consistently temporally upregulated and even temporally downregulated in these compartments during cold ischemia injury. Within the renal inner medulla, the leading-edge genes of the positively enriched energy metabolism pathways were related to various processes of mitochondrial machinery like *Atp5b* for ATP synthesis, *Cox6a1* (OXPHOS pathway), *Ppargc1a* for mitochondrial biogenesis (Thermogenesis pathway) and *Mdh1 for* TCA cycle pathway (Fig. 3H-K). (The complete list of leading-edge genes associated with the corresponding enriched molecular pathways are summarized in Table. S6). We performed compartment-specific qPCR to validate these observations using 4-5 animals per time point (Methods). Although we observe a comparatively higher expression of the energy metabolism related genes like *Atp5b*, *Cox6a1* and *Ppargc1a* (Fig. 3L-N) within the medulla (inner medulla and outer medulla combined) as compared to cortex throughout the cold ischemic phase, confirming compartmental differences, a consistent temporal trend was lacking. We speculate that this inconsistency might be resulting from the pooling of the outer and inner medulla tissue into a single group (called medulla) due to the limitations in manual surgical segmentation of the two compartments. Of note, in the normal kidney, the inner medulla, being in an oxygen lean environment, is known to primarily rely on anaerobic respiration while the cortical region (proximal tubules) is known to utilize OXPHOS owing to their high metabolic demand (*22*). However, the enrichment of OXPHOS and TCA cycle specifically within the inner medulla contrasts with this, suggestive of a potential metabolic reprogramming in response to the cold storage conditions.

To understand how OXPHOS could be sustained within a nutrient limited cold ischemic environment, we scrutinized significantly enriched metabolic pathways that can potentially generate metabolic substrates to drive the process. While most metabolic pathways such as fatty acid degradation (ID: mmu00071; genes: *Cpt1a, Acox1*, etc.), tryptophan metabolism (ID: mmu00380, genes: *Haao, Kmo, Gcdh*, etc.), and valine, leucine and isoleucine metabolism (ID: mmu00280 ; genes: *Dbt, Mccc1, Aldh6a1*, etc.) were negatively enriched within all the renal compartments, glycolysis/ gluconeogenesis (ID: mmu00010, genes: *Hk1, Pdha1, Pdhab, Pkm, Dlat,* etc.) was positively upregulated only within the inner medulla (Fig. S5A-E). Temporal upregulation of genes like *Pdha1*, *Pdhb*, *Dlat*, etc. within the inner medulla suggests potential coupling between glycolysis and TCA cycle via Acetyl-CoA intermediate (Fig. S5F-H). Consistently, we observed positive enrichment of HIF-1 signaling pathway (ID: mmu04066; genes: *Mapk1, Akt1, Vegfa*, etc.) within the inner medulla along with the temporal upregulation of glucose transporter gene *Slc2a1 (*Fig. S5I*)*. While the heightened glycolytic signature is consistent with previous studies demonstrating association between HIF-1 pathway and glycolytic metabolism (*23*, *24*), the co-enrichment of glycolytic and OXPHOS pathways within the cold ischemic renal inner medulla seems aberrant.

Unlike energy metabolism pathways which exhibited a compartment specific gene regulation, we observed several pathways that were regulated in a compartment agnostic manner indicative of pan-tissue effects. For instance, pathway related to reactive oxygen species (ID: mmu05208; genes: *Sod2*, etc.) was positively enriched across all compartments suggestive of oxidative stress (Fig. 3A-C, S6). Positive enrichment of pathways related to protein folding and quality control like Alzheimer disease (mmu05010), Huntington disease (mmu05016), prion disease (mmu05020), amyotrophic lateral sclerosis (mmu05014), and neurodegeneration (mmu05022), involving shared genes like *Hspa5, Creb3, Prnp, Psmd2, Psmd3, Psmd14*, etc (Fig. 3A-C). was observed. Finally, antigen processing and presentation pathway (ID: mmu04612, genes: *Ctsb, B2m, Psme, Cd74, H2-Aa,* etc.,) involving some genes related to major histocompatibility complex (MHC)-I and II was positively enriched across all compartments suggesting the

buildup of an immunogenic environment in response to cold ischemia injury (Fig. S7A-H). Collectively, both compartment-specific metabolic reprogramming and tissue-side pathological molecular changes were identified within cold ischemic renal tissue.

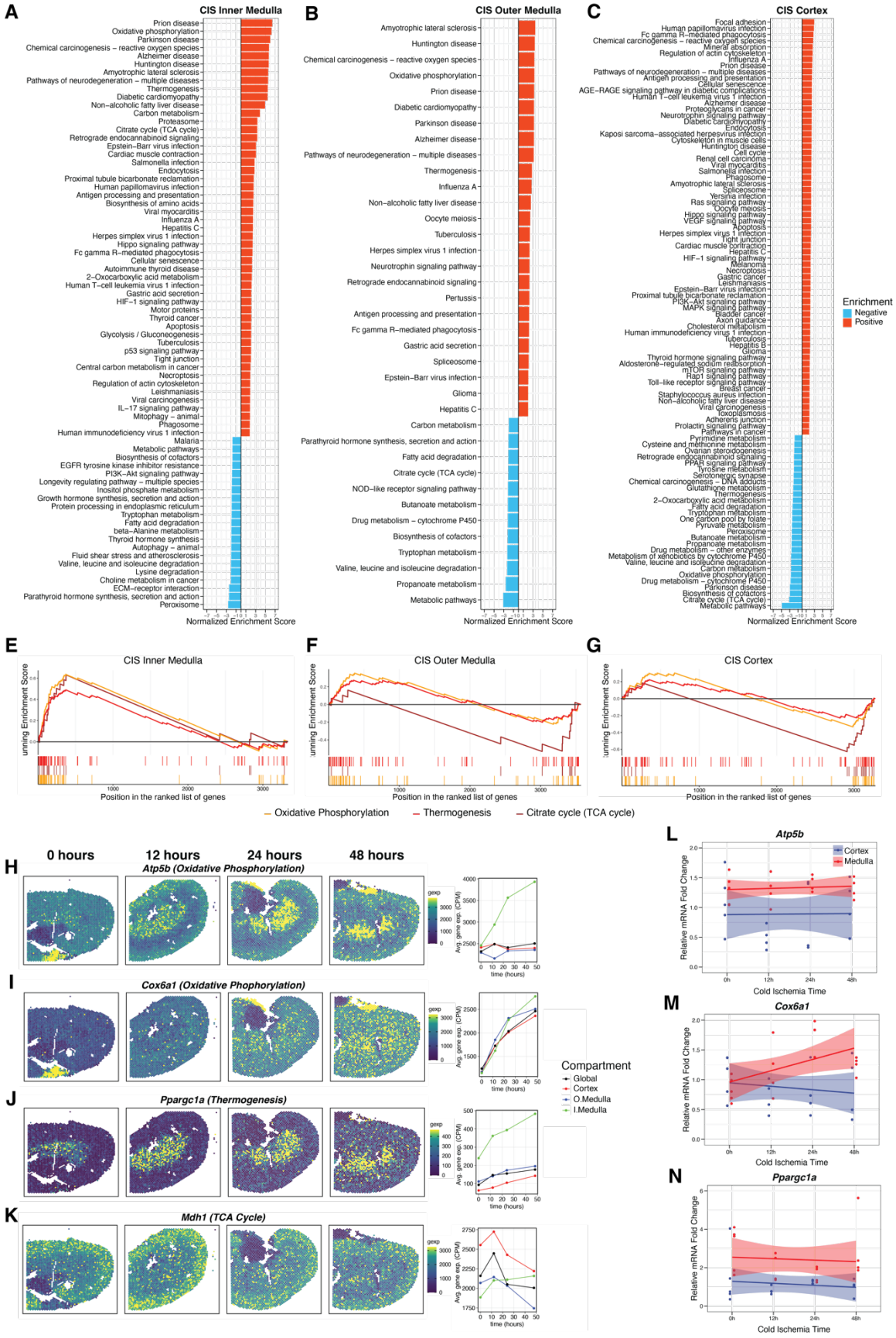
A
CIS Inner Medulla
Prion disease
Oxidative phosphorylation
Parkinson disease
Chemical carcinogenesis – reactive oxygen species
Alzheimer disease
Huntington disease
Amyotrophic lateral sclerosis
Pathways of neurodegeneration – multiple diseases
Thermogenesis
Diabetic cardiomyopathy
Non–alcoholic fatty liver disease
Carbon metabolism
Proteasome
Citrate cycle (TCA cycle)
Retrograde endocannabinoid signaling
Epstein–Barr virus infection
Cardiac muscle contraction
Salmonella infection
Endocytosis
Proximal tubule bicarbonate reclamation
Human papillomavirus infection
Antigen processing and presentation
Biosynthesis of amino acids
Viral myocarditis
Influenza A
Hepatitis C
Herpes simplex virus 1 infection
Hippo signaling pathway
Fc gamma R–mediated phagocytosis
Cellular senescence
Autoimmune thyroid disease
2–Oxocarboxylic acid metabolism
Human T–cell leukemia virus 1 infection
Gastric acid secretion
HIF–1 signaling pathway
Motor proteins
Thyroid cancer
Apoptosis
Glycolysis / Gluconeogenesis
Tuberculosis
p53 signaling pathway
Tight junction
Central carbon metabolism in cancer
Necroptosis
Regulation of actin cytoskeleton
Leishmaniasis
Viral carcinogenesis
IL–17 signaling pathway
Mitophagy – animal
Phagosome
Human immunodeficiency virus 1 infection
Malaria
Metabolic pathways
Biosynthesis of cofactors
EGFR tyrosine kinase inhibitor resistance
PI3K–Akt signaling pathway
Longevity regulating pathway – multiple species
Inositol phosphate metabolism
Growth hormone synthesis, secretion and action
Protein processing in endoplasmic reticulum
Tryptophan metabolism
Fatty acid degradation
beta–Alanine metabolism
Thyroid hormone synthesis
Autophagy – animal
Fluid shear stress and atherosclerosis
Valine, leucine and isoleucine degradation
Lysine degradation
Choline metabolism in cancer
ECM–receptor interaction
Parathyroid hormone synthesis, secretion and action
Peroxisome
Normalized Enrichment Score
B
CIS Outer Medulla
Amyotrophic lateral sclerosis
Huntington disease
Chemical carcinogenesis – reactive oxygen species
Oxidative phosphorylation
Prion disease
Diabetic cardiomyopathy
Parkinson disease
Alzheimer disease
Pathways of neurodegeneration – multiple diseases
Thermogenesis
Influenza A
Non–alcoholic fatty liver disease
Oocyte meiosis
Tuberculosis
Herpes simplex virus 1 infection
Neurotrophin signaling pathway
Retrograde endocannabinoid signaling
Pertussis
Antigen processing and presentation
Fc gamma R–mediated phagocytosis
Gastric acid secretion
Spliceosome
Epstein–Barr virus infection
Glioma
Hepatitis C
Carbon metabolism
Parathyroid hormone synthesis, secretion and action
Fatty acid degradation
Citrate cycle (TCA cycle)
NOD–like receptor signaling pathway
Butanoate metabolism
Drug metabolism – cytochrome P450
Biosynthesis of cofactors
Tryptophan metabolism
Valine, leucine and isoleucine degradation
Propanoate metabolism
Metabolic pathways
Normalized Enrichment Score
C
CIS Cortex
Focal adhesion
Human papillomavirus infection
Fc gamma R–mediated phagocytosis
Chemical carcinogenesis – reactive oxygen species
Mineral absorption
Regulation of actin cytoskeleton
Influenza A
Prion disease
Pathways of neurodegeneration – multiple diseases
Antigen processing and presentation
Cellular senescence
AGE–RAGE signaling pathway in diabetic complications
Human T–cell leukemia virus 1 infection
Alzheimer disease
Proteoglycans in cancer
Neurotrophin signaling pathway
Diabetic cardiomyopathy
Endocytosis
Kaposi sarcoma–associated herpesvirus infection
Cytoskeleton in muscle cells
Huntington disease
Cell cycle
Renal cell carcinoma
Viral myocarditis
Salmonella infection
Phagosome
Amyotrophic lateral sclerosis
Spliceosome
Yersinia infection
Ras signaling pathway
Oocyte meiosis
Hippo signaling pathway
VEGF signaling pathway
Apoptosis
Herpes simplex virus 1 infection
Tight junction
Cardiac muscle contraction
Hepatitis C
HIF–1 signaling pathway
Melanoma
Necroptosis
Gastric cancer
Leishmaniasis
Epstein–Barr virus infection
Proximal tubule bicarbonate reclamation
PI3K–Akt signaling pathway
MAPK signaling pathway
Bladder cancer
Axon guidance
Cholesterol metabolism
Human immunodeficiency virus 1 infection
Tuberculosis
Hepatitis B
Glioma
Thyroid hormone signaling pathway
Aldosterone–regulated sodium reabsorption
mTOR signaling pathway
Rap1 signaling pathway
Toll–like receptor signaling pathway
Breast cancer
Staphylococcus aureus infection
Non–alcoholic fatty liver disease
Viral carcinogenesis
Toxoplasmosis
Adherens junction
Prolactin signaling pathway
Pathways in cancer
Pyrimidine metabolism
Cysteine and methionine metabolism
Ovarian steroidogenesis
Retrograde endocannabinoid signaling
PPAR signaling pathway
Tyrosine metabolism
Serotonergic synapse
Chemical carcinogenesis – DNA adducts
Glutathione metabolism
Thermogenesis
2–Oxocarboxylic acid metabolism
Fatty acid degradation
Tryptophan metabolism
One carbon pool by folate
Pyruvate metabolism
Peroxisome
Butanoate metabolism
Propanoate metabolism
Drug metabolism – other enzymes
Metabolism of xenobiotics by cytochrome P450
Valine, leucine and isoleucine degradation
Carbon metabolism
Oxidative phosphorylation
Drug metabolism – cytochrome P450
Parkinson disease
Biosynthesis of cofactors
Citrate cycle (TCA cycle)
Metabolic pathways
Normalized Enrichment Score
Enrichment
Negative
Positive
E
CIS Inner Medulla
F
CIS Outer Medulla
G
CIS Cortex
Position in the ranked list of genes
Oxidative Phosphorylation
Thermogenesis
Citrate cycle (TCA cycle)
0 hours
12 hours
24 hours
48 hours
H
Atp5b (Oxidative Phosphorylation)
I
Cox6a1 (Oxidative Phophorylation)
J
Ppargc1a (Thermogenesis)
K
Mdh1 (TCA Cycle)
gexp
Avg. gene exp. (CPM)
time (hours)
Compartment
Global
Cortex
O.Medulla
I.Medulla
L
Atp5b
Cortex
Medulla
Relative mRNA Fold Change
Cold Ischemia Time
M
Cox6a1
N
Ppargc1a

Figure 3. Compartment-specific enrichment of molecular pathways within cold ischemic kidney tissue. Bar plots highlighting all the enriched molecular pathways that demonstrated similar temporal dynamics (enrichment: positive (red), negative (cyan)) within the corresponding **(A)** inner medulla **(B)** outer medulla and **(C)** cortex of cold ischemic injury renal tissue. Running enrichment score plots highlighting differential enrichment of molecular pathways related to energy metabolism: oxidative phosphorylation, citrate cycle (TCA cycle) and thermogenesis within the **(D)** inner medulla, **(E)** outer medulla and **(F)** cortex of the CIS renal tissue. Spatial gene expression plots and corresponding line plots demonstrating spatiotemporal dynamics of representative genes associated with the above enriched energy metabolism related pathways: **(H)** *Atp5b* and **(I)** *Cox6a1* (oxidative phosphorylation); **(J)** *Ppargc1a* (thermogenesis) and **(K)** *Mdh1* (TCA Cycle). Quantitative comparison of qPCR derived mRNA transcript levels of **(L)** *Atp5b,* **(M)** *Cox6a1* and **(N)** Ppargc1a between the cortex and medulla (inner medulla + outer medulla) of CIS renal tissue.

4. Comparison of cold ischemia and warm ischemia-reperfusion-induced AKI identifies overlapping molecular dynamics

To better understand the pathogenesis of renal cold ischemic injury, we next sought to compare its spatiotemporal transcriptomic dynamics with another ischemic injury setting. We therefore repeated the spatiotemporal analysis with a set of previously published ST datasets from a well-characterized murine model of warm ischemia-reperfusion-induced acute kidney injury (AKI) at various timepoints postinjury covering the peak phases of injury response (sham to 48 hours)(*17*). Our temporal analysis recapitulated putative AKI injury markers like *Havcr1, Lcn2 and Spp1* across all the compartments with *Spp1* demonstrating the sharpest change (linear regression slope) during the acute injury phase (Fig. S8A-C). Cross-compartmental analysis highlighted similar temporal transcriptional dynamics between the AKI

cortex and inner medulla (PCC=0.79, $p<0.05$, $R^2=0.63$) while the outer medulla and inner medulla were comparatively less similar (PCC=0.43, $p<0.05$, $R^2=0.19$) (Fig. S8D-F).

We next compared the temporal transcriptional dynamics between the corresponding compartments of the two injury models (i.e., CIS vs AKI). In contrast to CIS, in the warm ischemia-reperfusion-induced AKI model, while compartment-specific correlation analysis indicated a weak correlation between the inner medulla (PCC=0.04, $p>0.05$; R^2~0 (0.0019)) (Fig. 4A), comparatively stronger correlations were observed between the outer medulla (PCC=0.8, $p<0.05$; $R^2=0.64$) (Fig. 4B) and cortex (PCC=0.5, $p<0.05$; $R^2=0.25$) (Fig. 4C) of both the injuries. Interestingly, we observed *Spp1* upregulation across all compartments in both injury models with the inner medulla exhibiting the largest expression magnitude (Fig. 4A-C).

Thereafter, we performed gene set enrichment analysis to characterize pathways impacted in AKI as we did with CIS (Table S8, S9). In contrast to CIS, we observed that most molecular pathways demonstrated similar temporal trends across all the compartments (i.e., covarying pathways) with no divergent trends observed (Fig. S9A-F). Within the covarying pathways, pathways associated with energy metabolism like oxidative phosphorylation, citrate cycle (TCA cycle), fatty acid degradation, etc., demonstrated negative enrichment. In contrast, positive enrichment of both reparative processes like DNA replication (ID: mmu03030; genes: *Pold4, Pcna, Mcm2, Mcm7, Lig1*, etc.), PI3K-Akt signaling pathway (ID: mmu04151; genes: *Spp1, Hras, Cdk4, Cdk6, Pdgfra, Pdgfrb*, etc.) as well as pathological processes like apoptosis (ID: APOPTOSIS; genes: *Pea15a, Dap, Bax, Ifngr1, Anxa1*, etc.), epithelial-to-mesenchymal transition (or EMT) (ID: EPITHELIAL_MESENCHYMAL_TRANSITION; genes: *Spp1, Col1a1, Acta2, Fn1, Vim*, etc.), endoplasmic reticulum stress (ID: UNFOLDED_PROTEIN_FOLDING; genes: *Hsp90b1, Eif4ebp1, Calr, Eef2, Spcs3*, etc.), immune response (ID: ALLOGRAFT_REJECTION; genes: *Ikbkb, Ifngr1, Ifng2, Stat1, Ccr1, Ccr2, Tlr1, Ncf4*, etc.), etc., was observed, suggesting a diseased environment undergoing tissue repair. Of note, positive enrichment of coagulation pathway (ID: COAGULATION; genes: *Clu, Fgg, Rac1, Thbd, Plat*,

etc.) and complement pathway (ID: COMPLEMENT; genes: *C1qa, C1qc, C3*, etc.) hinted at potential endothelial dysfunction/vascular remodeling and immune-complex formation activating the complement (classical) pathway during reperfusion. Moreover, the enrichment of a multitude of viral response pathways such as hepatitis C (ID: mmu05160), Epstein-Barr virus infection (ID: mmu05169), and human papillomavirus (ID: mmu05165), involving shared genes like *Irf3, Stat1, Ifnar1, Ifnar2, Bax, Bak1*, etc., highlighted a heightened immunogenic environment. These findings suggest that AKI injury may induce similar pathological events across the whole renal tissue in a more compartment-agnostic manner compared to CIS. Lastly, processes like apoptosis, EMT, complement, vascular dysfunction, immune response are known to be associated with ischemia-reperfusion injury (*25*) further validating the ability of our computational workflow in identifying relevant temporal gene and pathway changes that accompany the pathogenesis of diseases like AKI.

Finally, we compared the enriched pathways between the two injury models in a compartment-specific manner (Fig. 4 D-F). For compartment-specific pathways exhibiting divergent trends between the two injury models, most were confined to the inner medulla. For instance, pathways related to glycolysis/gluconeogenesis (ID: mmu00010; genes: *Hk1, Aldoa, Dlat, Pdha1, Pdhb,* etc.), 2-oxocarboxylic acid metabolism (ID: mmu01210; genes: *Got2, Ogdh, Idh2, Idh3b,* etc.), and TCA cycle (ID: mmu00020; genes: *Mdh1, Mdh2, Sdha, Suclg2,* etc.) were positively enriched only within the CIS inner medulla while negatively enriched within the AKI inner medulla. This finding is consistent with the weak correlation observed between the inner medulla earlier (Fig. 4A).

Given that the AKI datasets belonged to tissue specimens from female C57BL/6 mice while the CIS datasets were from male C57BL/6 mice tissue, we next sought to evaluate whether these compartment-specific divergent transcriptional dynamics were driven by sexual dimorphism. To investigate this, we analyzed normal control kidneys (CTRL) and 24-hours warm ischemia reperfusion injury kidney tissues (AKI24) from male C57BL/6 mice (*18*). First, we observed that the presentation of AKI maker genes like

Havcr1, *Lcn2* and *Spp1* within the 24-hour male (AKI24) kidney tissues was very similar to that of female kidney specimens (AKI) at 12 and 48 hours (Fig. S8G-I). Next, we performed differential expression analysis between inner medulla compartment belonging to the CTRL and AKI24 kidneys. We observed that the leading genes: *Hk1, Dlat, Pdha1, Pdhb* (glycolysis/gluconeogenesis); *Got2, Ogdh, Idh2, Idh3b* (2-oxocarboxylic acid metabolism); *Mdh1, Mdh2, Sdha, Suclg2* (TCA cycle) associated with the divergent pathways identified earlier (CIS inner medulla vs AKI inner medulla), exhibited similar expression trend during AKI injury within the inner medulla of these male kidneys as what was previously identified in the female kidneys. In particular, genes previously identified to be downregulated over time within the inner medulla in AKI in the female kidneys were again identified as downregulated within the inner medulla of AKI24 compared to CTLR in the male kidneys. Likewise, genes previously identified to be upregulated in the female kidneys were such as AKI markers *Havcr1, Lcn2 and Spp1*, were again identified as upregulated in the male kidneys (Fig. S8J). The only exception was *Aldoa* demonstrating a slight potential divergence upregulation. The above observations highlight that, overall, the compartment-specific divergent transcriptional dynamics observed between CIS and AKI are likely not driven by sexual dimorphism.

In addition, we identified several pathways that displayed similar trend across all or specific compartments suggesting that the two injuries share some commonality at a transcriptomic level. For instance, metabolic pathways like fatty acid degradation (ID: mmu00071; genes: *Cpt1a, Ehhadh*, etc.,), tryptophan metabolism (ID: mmu00380; genes: *Aadat, Gcdh,* etc.), valine, leucine and isoleucine metabolism (ID: mmu00280; genes: *Dbt*, *Aldh6a1*, etc.) were negatively enriched (Fig. 4D-F) while viral response pathways like Hepatitis C (ID: mmu05160; genes: *Tnfrsf1a, Mavs, Tbk1, Stat1,* etc.) and Epstein-Barr virus infection (ID: mmu05169; genes: *B2m, Mavs, Cxcl10, Stat1, H2-D1, H2-Aa, Nfkb2,* etc.) were positively enriched in all the compartments (Fig.D-F, G-I, K-M) across both injury models. Intriguingly, we also observed positive enrichment of complement pathway within the outer medulla of both the injuries (Fig. 4J, N). Collectively, the transcriptomic presentation of both the injuries shared many molecular trends

across evaluated compartments, highlighting potential similarities in injury response across these distinct ischemic contexts and presenting implication in the poor clinical outcome associated with longer CIT.

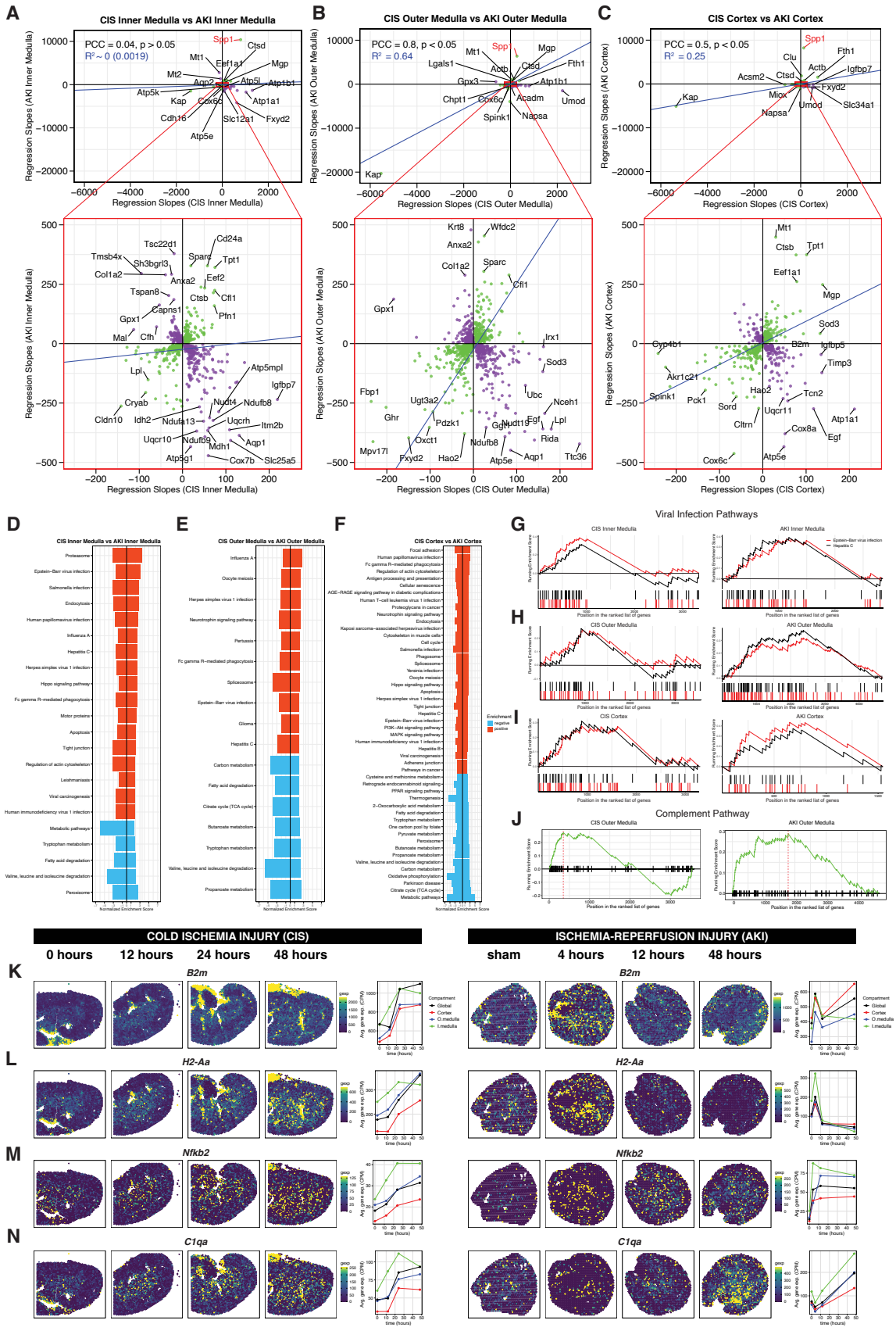
A
CIS Inner Medulla vs AKI Inner Medulla
PCC = 0.04, p > 0.05
R² ~ 0 (0.0019)
Regression Slopes (AKI Inner Medulla)
Regression Slopes (CIS Inner Medulla)
B
CIS Outer Medulla vs AKI Outer Medulla
PCC = 0.8, p < 0.05
R² = 0.64
Regression Slopes (AKI Outer Medulla)
Regression Slopes (CIS Outer Medulla)
C
CIS Cortex vs AKI Cortex
PCC = 0.5, p < 0.05
R² = 0.25
Regression Slopes (AKI Cortex)
Regression Slopes (CIS Cortex)
D
CIS Inner Medulla vs AKI Inner Medulla
E
CIS Outer Medulla vs AKI Outer Medulla
F
CIS Cortex vs AKI Cortex
Normalized Enrichment Score
Enrichment
negative
positive
G
Viral Infection Pathways
CIS Inner Medulla
AKI Inner Medulla
Epstein−Barr virus infection
Hepatitis C
H
CIS Outer Medulla
AKI Outer Medulla
I
CIS Cortex
AKI Cortex
J
Complement Pathway
CIS Outer Medulla
AKI Outer Medulla
Running Enrichment Score
Position in the ranked list of genes
COLD ISCHEMIA INJURY (CIS)
0 hours
12 hours
24 hours
48 hours
ISCHEMIA-REPERFUSION INJURY (AKI)
sham
4 hours
12 hours
48 hours
K
B2m
L
H2-Aa
M
Nfkb2
N
C1qa
Compartment
Global
Cortex
O.medulla
I.medulla
time (hours)
Avg. gene exp. (CPM)

Figure 4. Compartment-specific comparison of transcriptional dynamics between the CIS and AKI renal tissue. Scatter plots depicting the correlation analysis of the temporal transcriptional dynamics between the corresponding **(A)** inner medulla, **(B)** outer medulla and **(C)** cortex tissue compartments of the two renal injury models i.e., cold ischemic injury (CIS) and warm ischemia-reperfusion injury (AKI) kidney tissue. Genes exhibiting covarying (green) or divergent (purple) temporal trend within these compartments can be visualized along with their Pearson correlation coefficients (PCC) and linear regression slopes (blue line). Bar plots highlighting all the enriched molecular pathways that demonstrated similar temporal dynamics (enrichment: positive (red), negative (cyan)) within the corresponding **(D)** inner medulla, **(E)** outer medulla and **(F)** cortex of CIS and AKI renal tissue. Running enrichment score plots of positively enriched viral response like pathways like Epstein-Barr virus infection (red) and Hepatitis C (black) pathways within the corresponding **(G)** inner medulla, **(H)** outer medulla and **(I)** cortex of CIS and AKI renal tissue. **(J)** Running enrichment score plots of positively enriched complement pathway within the corresponding outer medulla of CIS and AKI renal tissue. Spatial gene expression plots and corresponding line plots demonstrating spatiotemporal dynamics of genes associated with the positively enriched Epstein-Barr virus infection pathway like **(K)** *B2m,* **(L)** *H2-Aa,* **(M)** *Nfkb2*; and complement pathway like **(N)** *C1qa* within both the CIS and AKI renal tissue.

5. Metabolic reprogramming mediated mitochondrial dysfunction may be implicated in cold ischemia injury

To summarize, our temporally-resolved spatial transcriptomics data and analyses have identified potential compartment-specific metabolic changes that arise in murine kidneys with increasing durations of cold ischemia. Notably, we identified two striking trends: (1) a metabolic switch to an oxygen demanding OXPHOS pathway within a hypoxic environment particularly within the inner medulla of the cold ischemic renal tissue and (2) concomitant pan-tissue downregulation of most metabolic intermediate generating

pathways (fatty acid degradation, tryptophan metabolism, valine, leucine and isoleucine metabolism, etc.) that can provide metabolites to drive OXPHOS (Fig. 5). These metabolic intermediates normally serve as substrates for the tricarboxylic acid (TCA) cycle, which in turn produces high-energy electron carriers (e.g., NADH and $FADH_2$) that drive the electron transport chain (ETC) and facilitate ATP generation via OXPHOS. The simultaneous upregulation of OXPHOS along with the downregulation of upstream metabolic intermediate pathways that supply its substrates thus presents a physiological paradox. We speculated that downregulation of metabolic intermediate pathways could reduce the production of high-energy electron carriers that fuel the ETC. Reduced ETC activity may lead to a loss of proton gradient across the mitochondrial membrane and may be a source of mitochondrial dysfunction. Mitochondrial dysfunction has been implicated in AKI due to the increased oxidative stress generated in the damaged mitochondria of proximal tubule cells and has been shown to trigger the onset of injury responses such as mitochondrial membrane depolarization-induced mitophagy (*26–28*).

To check for mitochondrial dysfunction during cold ischemia injury, we probed for one of the putative effector molecules involved in mitophagy, PTEN-induced kinase 1 (*Pink1*), which is known to be upregulated in response to mitochondrial distress and initiate the mitophagy faciliated clearance of damaged mitochondria (*29*). Using our ST data, we observe that *Pink1* is temporally upregulated with increasing duration of cold ischemia across all compartments (Fig. S10A), though pathway analysis identified positive enrichment of mitophagy (ID: mmu04137, genes: *Pink1, Becn1, Tbk1, Tfeb, etc*.) as unique to the CIS inner medulla (Fig. S10B-E)). To further validate these transcriptional trends, we again performed qPCR. Consistent with our ST findings, qPCR revealed that *Pink1* is upregulated with increasing CIT in the medulla (Fig. S10F). Consistent with our pathway analysis, *Pink1* expression within the cortex did not exhibit the same upregulation with prolonged CIT. In general, this spatial divergence in *Pink1* expression suggests that mitophagy may be differentially regulated across renal compartments during cold ischemia injury. Collectively, these finding point towards a potential dysfunction in the mitochondrial

machinery which might be the result of a compartment-specific aberrant metabolic reprogramming within a cold ischemic environment.

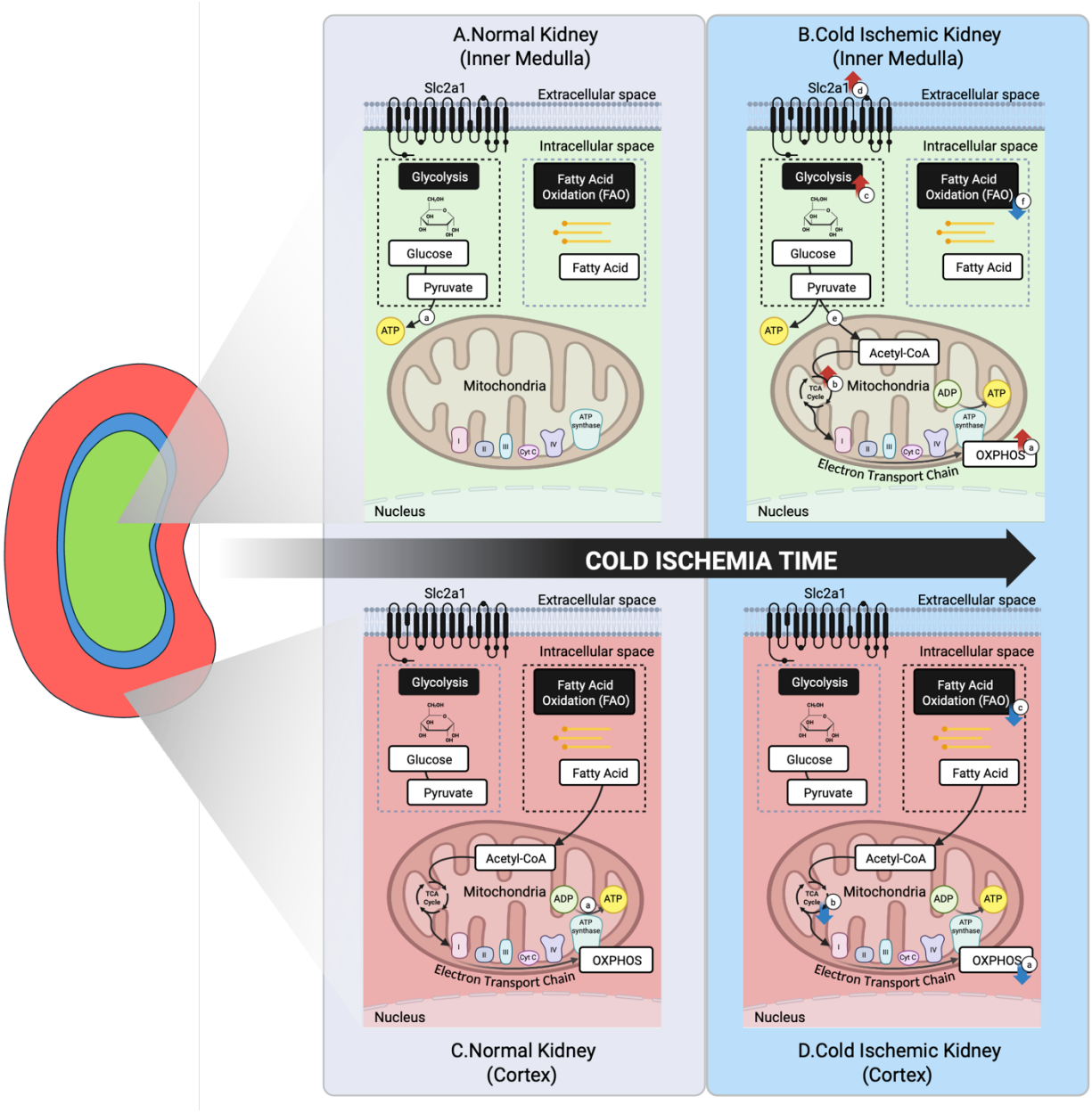

Figure 5. Summary of prolonged cold ischemia injury induced compartment-specific metabolic changes in murine kidneys. (A) Normal kidney (inner medulla): The inner medulla of normal kidney relies primarily on glycolysis pathway (black dashed lines) to (a) generate ATP to meet its low metabolic demand. **(B)** Cold ischemic kidney (inner medulla): During cold ischemia injury, molecular pathways related to energy

metabolism like (a) OXPHOS and (b) TCA cycle were positively enriched (red arrows). Enrichment of (c) glycolysis pathway and (d) glucose transporter gene *Slc2a1* were positively enriched and upregulation of genes like *Dlat, Pdha1, Pdhb* suggested (e) coupling of glycolysis and TCA cycle. Finally, (f) negative enrichment (blue arrows) of fatty acid oxidation (FAO) pathway (blue dashed lines) was observed. Simultaneous positive enrichment of OXPHOS and glycolysis with negative enrichment of fatty acid oxidation suggests aberrant metabolic reprogramming with the inner medulla of cold ischemic kidneys. **(C)** Normal kidney (cortex): The cortex of normal kidney relies primarily on OXPHOS to generate (a) ATP to meet its high energy demand with FAO (black dashed lines) providing the required metabolic intermediates to drive OXPHOS. **(D)** Cold ischemic kidney (cortex): Both (a) OXPHOS and (b) TCA cycle as well as (c) FAO were negatively enriched during cold ischemia injury. This trend was also observed within the cortex of AKI renal tissue wherein OXPHOS, TCA cycle and FAO were observed to be negatively enriched. (Different colors represent different compartments of the renal tissue: inner medulla (green), outer medulla (blue) and cortex (red)). Created with BioRender.com

Discussion

Long durations of cold preservation storage results in cold ischemia injury and contributes to worse graft outcomes (*6*). However, the molecular events during the pathogenesis of this injury are incompletely understood, particularly in the medulla of the kidney less amenable to safe percutaneous or wedge biopsy sampling. We therefore performed a full transcriptome spatial characterization of cold ischemia in murine kidneys (0-48 hours) using ST with 10x Visium. Using a data driven computational analysis approach, we identified temporal regulation of genes within transcriptionally distinct compartments of the kidney tissue, which allowed us to study regulation of genes and associated molecular pathways within the individual compartments of the cold ischemia tissue. We further extended this workflow to enable comparison with early injury response in warm ischemia-reperfusion-induced AKI.

Our analysis identified several genes that demonstrated significant time dependent regulation within the different compartments of cold ischemic kidneys. These genes were associated with a wide range of processes but importantly energy metabolism, oxidative stress and immune response. In general, all the compartments elevated their expression of genes related to antigen presentation protein complexes (i.e., MHC-I, MHC-II) and displayed heightened molecular signatures of an immunogenic environment reminiscent of a response to viral infection. While metabolic pathways were downregulated across all compartments, the inner medulla unexpectedly demonstrated elevated expression of OXPHOS pathway. The upregulation of OXPHOS pathway within the oxygen lean renal inner medulla, which relies on anaerobic respiration, suggests potential metabolic reprogramming. However, the limited availability of oxygen along with downregulation of essential metabolic substrates to drive OXPHOS contributes to oxidative stress mediated mitochondrial dysfunction and potentially the subsequent induction of an allo-immunogenic environment.

Comparative analysis between the cold ischemia injury and warm ischemia-reperfusion-induced AKI settings in a compartment specific manner identified many covarying as well as divergent trends. Both the injured tissue displayed elevated molecular signatures of viral response over time indicating the presence of an immunogenic environment, and a marked decrease in metabolism of many relevant substrates. Moreover, cross-compartment correlation analysis highlighted that warm ischemia-reperfusion-induced AKI evoked similar transcriptional response across all compartments while cold ischemia induced molecular changes were more compartment specific. This was particularly evident within the spatiotemporal molecular presentation of the OXPHOS pathway between the two injuries. These observations suggest that even though the two injuries have different etiologies and involve distinct molecular pathways within the different tissue compartments, they may still share some commonality in their spatiotemporal transcriptomic presentation.

Although our current study brings in new molecular insights into the pathogenesis of cold ischemic injury within the kidney, there are limitations which may be addressed in future studies. First, the lack of single cell resolution in our spatial transcriptomic profiling limits our understanding of the cell-type specific effects within the different compartments during cold ischemia injury. Single-cell resolution ST platforms like Xenium (*30*) or MERFISH (*31*) could be utilized to perform such cellular characterization, though they are limited in the number of genes they can profile simultaneously and therefore should be informed by full-transcriptome characterizations such as this study. Next, our findings rely on observations made from computational analysis of ST data derived from a single sample per timepoint (i.e., n=1 per cold ischemia duration) experimental design. We employed qPCR with a larger animal cohort (n=4-5 per timepoint) to check the validity of key findings from CIS data. Moreover, results from our AKI analyses were consistent with existing literature related to acute kidney injury despite also being limited to a single sample per timepoint. Although this underscores the validity of the computational workflow, the experimental rigor would benefit from a larger sample size. We also acknowledge that static cold storage injury likely has differences from newer storage approaches like hypothermic pulsatile perfusion and normothermic machine perfusion.

We acknowledge that our comparison of CIS (in male mice) and AKI (in female mice) datasets is confounded by potential sexual dimorphism. However, we note that known sexual dimorphism in renal tissue has been primarily confined to the cortical region (with strong differences observed in the S3 segment of proximal tubule) of the kidney (*21*), whereas the differences we observed were within the inner medulla. Still, the effect of sexual dimorphism on the response to cold ischemia injury presents an opportunity for future investigation.

Finally, there are logistical differences between the current experimental design and a clinical scenario wherein deceased donor kidneys undergo nephrectomy first and perfused *ex vivo* using renal arteries whereas the murine kidneys in the current study were perfused through the hepatic portal vein

first and harvested thereafter. Given that murine arteries present size-related challenges during perfusion, we anticipate large animal models like porcine models can be strategized to recapitulate the clinical scenario more accurately in the future.

We believe that these findings will serve as a basis for future studies enhancing the clinical decision-making process related to selection and reduced discard of deceased donor kidneys. For instance, kidney biopsies are routinely examined for underlying pathologies primarily within the cortical region containing the proximal tubules as they are sensitive to oxidative stress and susceptible to cellular injury. As such, pathologies developing deep within the tissue such as in the renal inner medullary region remain undetected. This might not be an issue in an AKI setting where we found the cortex and inner medulla to exhibit strong positive correlation, mirroring each other's temporal molecular dynamics. However, in a cold ischemia setting where the cortex and inner medulla demonstrated very weak correlation it might be worth evaluating the potential benefit of examining the inner medulla as part of the clinical routine. Furthermore, comparison of static cold ischemia vs. cold perfused vs. normothermic perfusion is also needed in the future in this evolving field. In order to make our data more accessible and understandable beyond those with expertise in spatial transcriptomic analysis, we also developed an interactive online browser at https://jef.works/vitessce-cold-ischemia/. Overall, we anticipate such spatiotemporally resolved molecular comparative analysis will enhance our understanding of biological processes underlying disease pathogenesis to help elucidate novel therapeutics in the future.

Materials and Methods

Cold Ischemia Model and Kidney Collection:

7-8 weeks old C57BL/6 male mice were anesthetized via isoflurane inhalation and perfused with ice-cold University of Wisconsin (UW) solution through the hepatic portal vein using a 10 cc syringe with a 25G needle. To facilitate circulation, the inferior vena cava below the liver was incised, enabling whole-body perfusion with UW solution. Following perfusion, the kidneys were harvested and immediately stored in UW solution at 4°C for 0, 12, 24, or 48 hours to induce cold ischemia. After the designated cold ischemia period, the kidneys were removed from the UW solution and fixed in 10% phosphate-buffered formalin for a minimum of 48 hours.

Sample preparation for spatial transcriptomics characterization:

To profile the global spatial transcriptome after cold ischemia at 0, 12, 24, and 48 hours, formalin fixed kidneys were cut sagittally, embedded in paraffin and sectioned under RNase free conditions. Kidney section (5mm) were placed on a positively charged glass slide, H&E stained and scanned. One kidney section from each timepoint was placed on 10x Visium FFPE (formalin fixed paraffin embedded) slide using CytAssist instrument. Adjacent sections (20 mm) were used for RNA quality assessment and samples with RQN value 7 were used for spatial transcriptomic analysis. Tissue processing and downstream analyses were achieved by adopting the following 10x Genomics protocols without any alteration: (1) Visium CytAssist Spatial Gene Expression for FFPE (CG000520, Revision B) for deparaffinization, staining, decrosslinking and imaging of slides. (2) “Sequencing” sections of the Visium CytAssist Spatial Gene Expression Reagent Kits User Guide (CG000495) for hybridization. The CytAssist libraries were sequenced using a Novaseq 6000 sequencer. Gene expression counts and spot positions were obtained using the SpaceRanger pipeline (v2.0.1) for downstream analysis.

Public data access:

Previously published 10x Visium spatial transcriptomics datasets from coronal sections of female murine kidneys with bilateral ischemia reperfusion injury (ID: AKI (n=5), timepoints: sham, 4, 12, 48 hours and 6 weeks) (*17*) were obtained from the Gene Expression Omnibus (GEO) under accession GSE182939. Likewise, previously published 10x Visium spatial transcriptomics (ST) datasets sections of sagittal sections of normal control male murine kidneys (ID: CTRL(n=4)) and of male murine kidneys with bilateral ischemia reperfusion injury (ID: AKI24 (n=4), timepoint: 24 hours (all specimens)) were obtained from the authors (*18*). All datasets were accessed as gene counts matrices and spatial positions in preprocessed h5 files.

Quality Control and Processing:

Any 10x Visium spots with less than 100 counts were removed. This resulted in a total of 44,816 spots belonging to all the 17 different spatial transcriptomics datasets. R statistical software (version 4.3.1 (2023-06-16)) was used for this purpose and all the computational analyses hereafter.

Data Integration, Batch Correction and Graph Based Clustering:

For data integration, for each of the individual ST dataset (prior to CPM normalization), we removed genes with less than 10 reads across all spots. Thereafter, we feature selected for over-dispersed genes in each dataset using the getOverdispersedGenes() function from MERINGUE (*32*) To mitigate sample-specific effects, we identified genes that were overdispersed in at least 2 datasets resulting in 1,378 final shared overdispsersed genes. Using these over-dispersed genes, the top 30 principal components (PCs) were identified. Batch correction was performed on the PCs to obtain harmonized PCs using the HarmonyMatrix() function (parameters: theta = 10, lambda = 0.05) from Harmony (*19*). Low-dimensional 2D embeddings of the initial and harmonized PCs were obtained using tSNE (*33*). Graph-based Louvain clustering was performed on the harmonized PCs to identify transcriptionally similar spots using

getClusters() function (parameters: k=100) from MERINGUE (*32*). Thereafter, for normalization purposes and subsequent linear regression analysis (covered in next section), the gene list was restricted to 19,454 unique genes that were shared across all 17 ST datasets.

Linear regression modeling:

Gene count matrices of CIS tissue specimens containing 19,454 unique shared genes (rows) at each timepoint 0, 12, 24 and 48 hours were subset into smaller compartment-specific matrices based on the annotations obtained from harmonized clustering. This resulted in generation of 3 matrices per timepoint capturing all the spots within the inner medulla, outer medulla, and cortex compartments respectively. Thereafter, we performed CPM (counts per million) normalization on the gene counts matrices to obtain count-normalized matrices using normalizeCounts() function from MERINGUE (*32*). To avoid over-representation from any particular compartment (especially the cortex), 190 random spots were sampled for each of these matrices belonging to the 3 compartments (per timepoint) to perform compartment-specific linear regression at each timepoint. lmfit() function from limma (*34*) package was used to perform linear regression with time (encoded as $\log_e$(hours+1)) as the independent variable (x) and count-normalized gene counts as the dependent variable (y). Adjusted p-value (adj. $p < 0.05$) was used as a criterion to select the genes whose expression had significant temporal association (reflected by the magnitude of linear regression slope with unit as: CPM normalized read/$\log_e$(hours+1)). Similar procedure was implemented on AKI tissue specimens at timepoints (0 (sham), 4, 12 and 48 hours).

Gene Set Enrichment Analysis:

These genes with significant temporal association identified through linear regression were ordered based on the strength of their temporal association (linear regression slopes). These genes were assigned a value which reflected their rank in the ordered list such that temporally upregulated genes received a positive

score while temporally downregulated genes received a negative score. Thereafter, gene set enrichment analysis was performed on the ordered list of genes along with their assigned values using gseKEGG() function from ClusterProfiler (*35*) package and GSEA() function from Msigdbr (*36*) package to identify enriched KEGG and Hallmark (gene set of Msigdbr) molecular pathways respectively. Adjusted p-value (adj. $p<0.05$) was used as a cut-off criterion to select significantly enriched molecular pathways. Running enrichment score plots were plotted using gseaplot() and gseaplot2() functions from enrichplot (*37*) package.

Compartmental correlation analysis and linear regression:

Correlation analysis of the temporal transcriptomic dynamics between the different compartments was performed using cor.test() function in R to obtain Pearson correlation coefficient (PCC) and p-value. Linear regression was performed using lm() function in R and summary function was used to obtain the R^2 value.

Differential Expression Analysis:

Differential expression analysis was performed to identify top marker genes of inner medulla, outer medulla, and cortex compartments. Briefly, count matrices (raw counts) belonging to all the 17 ST datasets were split into three groups based on the labels (from earlier assigned compartmental annotations) of the spots. Thereafter, differential expression analysis was performed between the interest group and the other two groups pooled together into one group using DESeq2 (*38*). Top 30 genes based on their log2 fold change (and adjusted p-value<0.05) from each of the compartments were identified and plotted as heatmaps. Differential expression was also performed between the inner medulla compartment of all 4 kidney tissue specimens belonging to normal control kidneys (CTRL) and 4 warm ischemia reperfusion injury (AKI24) to evaluate consistency with linear regression modeling.

RNA isolation and qPCR:

Kidney cortex and medulla (inner + outer medulla) were collected as previously described (*39*) .)Total RNA was isolated from samples using a QIAshredder (Qiagen, Valencia, CA, Cat.No.79654) and a RNeasy Mini kit (Qiagen, Cat.No.74104) and reverse transcribed using High-Capacity cDNA Reverse Transcription Kit (Applied Biosystems, Foster City, CA, Cat.No. 4368814). Real-time PCR was performed in QuantStudio 12K Flex (Applied Biosystems, Foster City, CA) using the SYBR Green PCR master mix (Applied biosystems, Cat.No. 4309155). β-actin served as the reference gene and the relative fold expression values were calculated using a DD cycle threshold method. The primer sequences for genes are listed below:

Genes	Forward primer	Reverse primer
Actb	GTGACGTTGACATCCGTAAAGA	GCCGGACTCATCGTACTCC
Atp5b	GCAAGGCAGGGACAGCAGA	CCCAAGGTCTCAGGACCAACA
Cox6a1	CAACGTGTTCCTCAAGTCGCGG	GCCAGGTTCTCTTTACTCATC
Pink1	TTCTTCCGCCAGTCGGTAG	CTGCTTCTCCTCGATCAGCC
Ppargc1a	CCCTGCCATTGTTAAGACC	TGCTGCTGTTCCTGTTTTC

Code availability:

Code to reproduce the analyses and results of this study is available on GitHub at: https://github.com/ssingh95jhu/Cold_Ischemia_Injury_Molecular_Characterization

An interactive browser made using Vitessce (*40*) available at https://jef.works/vitessce-cold-ischemia/ with source code at https://github.com/JEFworks-Lab/vitessce-cold-ischemia

Data availability:

Count matrices, spatial positions, and H&E images for the cold ischemia Visium datasets generated in this study have been deposited in a Zenodo repository at https://doi.org/10.5281/zenodo.15359609

Acknowledgements

This material is based upon work supported by the National Institute of General Medical Sciences of the National Institutes of Health under Award Number R35-GM142889 (SS, JF) and the National Science Foundation under Grant No. 2047611 (DV, JF). H.R. and S.N. were supported by NIH/NIDDK grants (R01DK132278, R01DK123342, U54DK137331) and the Kidney precision medicine project biomarker award.

Contributions

J.F. and H.R. conceptualized the study. S.S. led the data analysis, interpretation, and writing under the guidance of J.F. and with input from S.K.P., R.M., S.N., and H.R. S.K.P., R.M. and S.N. performed the cold ischemia protocol, kidney tissue collection, sectioning and tissue processing for spatial transcriptomics under the guidance of Z.S. and H.R. S.K.P., R.M. and S.N. led the qPCR validation under the guidance of H.R. D.V. developed the web application under the guidance of S.S. and J.F. All authors contributed to the writing of the manuscript. All authors approved the final manuscript.

References:

1. Centers for Medicare & Medicaid Services (Accessed: March 2025), Increasing Organ Transplant Access (IOTA) Model. https://www.cms.gov/priorities/innovation/innovation-models/iota.
2. L. Heylen, J. Pirenne, M. Naesens, B. Sprangers, I. Jochmans, "Time is tissue"—A minireview on the importance of donor nephrectomy, donor hepatectomy, and implantation times in kidney and liver transplantation. *American Journal of Transplantation* **21**, 2653–2661 (2021).
3. A. M. Placona, C. Humphries, C. Curran, W. Ambroise, J. P. Orlowski, K. Gauntt, J. Wainright, Association of Transit Time With Cold Ischemic Time in Kidney Transplantation. *JAMA Netw Open* **4**, e2141108 (2021).
4. J. F. McAnulty, Hypothermic organ preservation by static storage methods: Current status and a view to the future. *Cryobiology* **60**, S13–S19 (2010).
5. A. K. Salahudeen, Cold ischemic injury of transplanted kidneys: new insights from experimental studies. *American Journal of Physiology-Renal Physiology* **287**, F181–F187 (2004).
6. A. Debout, Y. Foucher, K. Trébern-Launay, C. Legendre, H. Kreis, G. Mourad, V. Garrigue, E. Morelon, F. Buron, L. Rostaing, N. Kamar, M. Kessler, M. Ladrière, A. Poignas, A. Blidi, J.-P. Soulillou, M. Giral, E. Dantan, Each additional hour of cold ischemia time significantly increases the risk of graft failure and mortality following renal transplantation. *Kidney Int* **87**, 343–349 (2015).
7. A. K. Salahudeen, H. Huang, P. Patel, J. K. Jenkins, MECHANISM AND PREVENTION OF COLD STORAGE-INDUCED HUMAN RENAL TUBULAR CELL INJURY12. *Transplantation* **70**, 1424–1431 (2000).
8. A. K. Salahudeen, H. Huang, M. Joshi, N. A. Moore, J. K. Jenkins, Involvement of the Mitochondrial Pathway in Cold Storage and Rewarming-Associated Apoptosis of Human Renal Proximal Tubular Cells. *American Journal of Transplantation* **3**, 273–280 (2003).
9. A. K. Salahudeen, Cold ischemic injury of transplanted kidneys: new insights from experimental studies. *American Journal of Physiology-Renal Physiology* **287**, F181–F187 (2004).
10. A. R. Krishnan, G. Wong, J. R. Chapman, P. T. Coates, G. R. Russ, H. Pleass, C. Russell, B. He, W. H. Lim, Prolonged Ischemic Time, Delayed Graft Function, and Graft and Patient Outcomes in Live Donor Kidney Transplant Recipients. *American Journal of Transplantation* **16**, 2714–2723 (2016).
11. L. Kayler, X. Yu, C. Cortes, M. Lubetzky, P. Friedmann, Impact of Cold Ischemia Time in Kidney Transplants From Donation After Circulatory Death Donors. *Transplant Direct* **3**, e177 (2017).
12. J. Gill, C. Rose, Y. Joffres, M. Kadatz, J. Gill, Cold ischemia time up to 16 hours has little impact on living donor kidney transplant outcomes in the era of kidney paired donation. *Kidney Int* **92**, 490–496 (2017).
13. G. K. Dube, C. Brennan, S. A. Husain, R. J. Crew, M. C. Chiles, D. J. Cohen, S. Mohan, Outcomes of kidney transplant from deceased donors with acute kidney injury and

prolonged cold ischemia time - a retrospective cohort study. *Transplant International* **32**, 646–657 (2019).
14. C. G. Williams, H. J. Lee, T. Asatsuma, R. Vento-Tormo, A. Haque, An introduction to spatial transcriptomics for biomedical research. *Genome Med* **14**, 68 (2022).
15. M. Cheng, Y. Jiang, J. Xu, A.-F. A. Mentis, S. Wang, H. Zheng, S. K. Sahu, L. Liu, X. Xu, Spatially resolved transcriptomics: a comprehensive review of their technological advances, applications, and challenges. *Journal of Genetics and Genomics* **50**, 625–640 (2023).
16. L. Atta, J. Fan, Computational challenges and opportunities in spatially resolved transcriptomic data analysis. *Nat Commun* **12**, 5283 (2021).
17. E. E. Dixon, H. Wu, Y. Muto, P. C. Wilson, B. D. Humphreys, Spatially Resolved Transcriptomic Analysis of Acute Kidney Injury in a Female Murine Model. *Journal of the American Society of Nephrology* **33**, 279–289 (2022).
18. S. Gharaie, K. Lee, K. Noller, E. K. Lo, B. Miller, H. J. Jung, A. M. Newman-Rivera, J. T. Kurzhagen, N. Singla, P. A. Welling, J. Fan, P. Cahan, S. Noel, H. Rabb, Single cell and spatial transcriptomics analysis of kidney double negative T lymphocytes in normal and ischemic mouse kidneys. *Sci Rep* **13**, 20888 (2023).
19. I. Korsunsky, N. Millard, J. Fan, K. Slowikowski, F. Zhang, K. Wei, Y. Baglaenko, M. Brenner, P. Loh, S. Raychaudhuri, Fast, sensitive and accurate integration of single-cell data with Harmony. *Nat Methods* **16**, 1289–1296 (2019).
20. M. S. Balzer, T. Rohacs, K. Susztak, How Many Cell Types Are in the Kidney and What Do They Do? *Annu Rev Physiol* **84**, 507–531 (2022).
21. A. Ransick, N. O. Lindström, J. Liu, Q. Zhu, J.-J. Guo, G. F. Alvarado, A. D. Kim, H. G. Black, J. Kim, A. P. McMahon, Single-Cell Profiling Reveals Sex, Lineage, and Regional Diversity in the Mouse Kidney. *Dev Cell* **51**, 399-413.e7 (2019).
22. A. J. Clark, S. M. Parikh, Mitochondrial Metabolism in Acute Kidney Injury. *Semin Nephrol* **40**, 101–113 (2020).
23. R. Lan, H. Geng, P. K. Singha, P. Saikumar, E. P. Bottinger, J. M. Weinberg, M. A. Venkatachalam, Mitochondrial Pathology and Glycolytic Shift during Proximal Tubule Atrophy after Ischemic AKI. *Journal of the American Society of Nephrology* **27**, 3356–3367 (2016).
24. G. Schley, B. Klanke, J. Schödel, F. Forstreuter, D. Shukla, A. Kurtz, K. Amann, M. S. Wiesener, S. Rosen, K.-U. Eckardt, P. H. Maxwell, C. Willam, Hypoxia-Inducible Transcription Factors Stabilization in the Thick Ascending Limb Protects against Ischemic Acute Kidney Injury. *Journal of the American Society of Nephrology* **22**, 2004–2015 (2011).
25. M. Salvadori, G. Rosso, E. Bertoni, Update on ischemia-reperfusion injury in kidney transplantation: Pathogenesis and treatment. *World J Transplant* **5**, 52 (2015).
26. G. P. Kaushal, S. V. Shah, Autophagy in acute kidney injury. *Kidney Int* **89**, 779–791 (2016).
27. D. Bhatia, A. Capili, M. E. Choi, Mitochondrial dysfunction in kidney injury, inflammation, and disease: Potential therapeutic approaches. *Kidney Res Clin Pract* **39**, 244–258 (2020).

28. M.-J. Kim, C. J. Oh, C.-W. Hong, J.-H. Jeon, Comprehensive overview of the role of mitochondrial dysfunction in the pathogenesis of acute kidney ischemia-reperfusion injury: a narrative review. *Journal of Yeungnam Medical Science* **41**, 61–73 (2024).
29. C. Tang, H. Han, M. Yan, S. Zhu, J. Liu, Z. Liu, L. He, J. Tan, Y. Liu, H. Liu, L. Sun, S. Duan, Y. Peng, F. Liu, X.-M. Yin, Z. Zhang, Z. Dong, PINK1-PRKN/PARK2 pathway of mitophagy is activated to protect against renal ischemia-reperfusion injury. *Autophagy* **14**, 880–897 (2018).
30. 10X Genomics (Accessed: March 2025), Xenium Platform, *https://www.10xgenomics.com/platforms/xenium*.
31. K. H. Chen, A. N. Boettiger, J. R. Moffitt, S. Wang, X. Zhuang, Spatially resolved, highly multiplexed RNA profiling in single cells. *Science (1979)* **348** (2015).
32. B. F. Miller, D. Bambah-Mukku, C. Dulac, X. Zhuang, J. Fan, Characterizing spatial gene expression heterogeneity in spatially resolved single-cell transcriptomic data with nonuniform cellular densities. *Genome Res* **31**, 1843–1855 (2021).
33. Jesse H. Krijthe (2015), Rtsne: T-Distributed Stochastic Neighbor Embedding using a Barnes-Hut Implementation, *https://github.com/jkrijthe/Rtsne*.
34. M. E. Ritchie, B. Phipson, D. Wu, Y. Hu, C. W. Law, W. Shi, G. K. Smyth, limma powers differential expression analyses for RNA-sequencing and microarray studies. *Nucleic Acids Res* **43**, e47–e47 (2015).
35. T. Wu, E. Hu, S. Xu, M. Chen, P. Guo, Z. Dai, T. Feng, L. Zhou, W. Tang, L. Zhan, X. Fu, S. Liu, X. Bo, G. Yu, clusterProfiler 4.0: A universal enrichment tool for interpreting omics data. *The Innovation* **2**, 100141 (2021).
36. I. Dolgalev, msigdbr: MSigDB Gene Sets for Multiple Organisms in a Tidy Data Format. [Preprint] (2018). https://doi.org/10.32614/CRAN.package.msigdbr.
37. Yu G (2025), enrichplot: Visualization of Functional Enrichment Result. R package version 1.26.6, *https://yulab-smu.top/biomedical-knowledge-mining-book/*.
38. M. I. Love, W. Huber, S. Anders, Moderated estimation of fold change and dispersion for RNA-seq data with DESeq2. *Genome Biol* **15**, 550 (2014).
39. R. A. Fenton, A. Flynn, A. Shodeinde, C. P. Smith, J. Schnermann, M. A. Knepper, Renal Phenotype of UT-A Urea Transporter Knockout Mice. *Journal of the American Society of Nephrology* **16**, 1583–1592 (2005).
40. M. S. Keller, I. Gold, C. McCallum, T. Manz, P. V. Kharchenko, N. Gehlenborg, Vitessce: integrative visualization of multimodal and spatially resolved single-cell data. *Nat Methods* **22**, 63–67 (2025).

Spatiotemporal transcriptomic analysis during cold ischemic injury to the murine kidney reveals compartment-specific changes

Supplemental Figures:

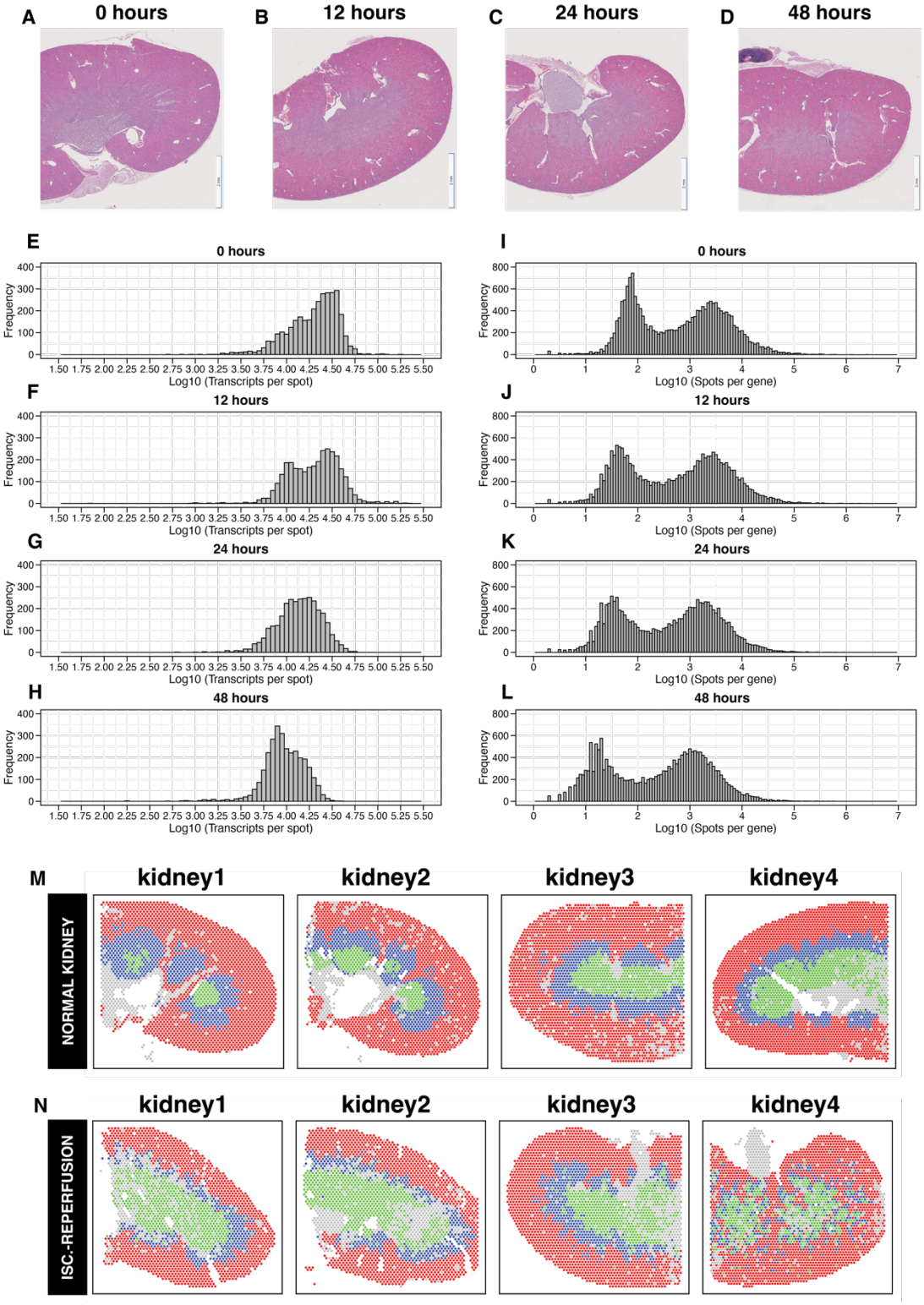

Figure S1. Tissue specimens and quality control of cold ischemia injury kidneys. H&E-stained images of kidney tissue specimens subjected to **(A)** 0 hours **(B)** 12 hours **(C)** 24 hours and **(D)** 48 hours of cold ischemia injury. Histograms depicting distribution of **(E-H)** transcripts per spot and **(I-L)** spots per gene at time points 0 hours, 12 hours, 24 hours and 48 hours of cold ischemia injury respectively. Annotations highlighting the different compartments namely cortex (red), outer medulla (blue), inner medulla (green) and other (gray), within the normal control (CTRL) kidneys (**M**) and 24-hours warm ischemia reperfusion (AKI24) injury (**N**) tissue specimens.

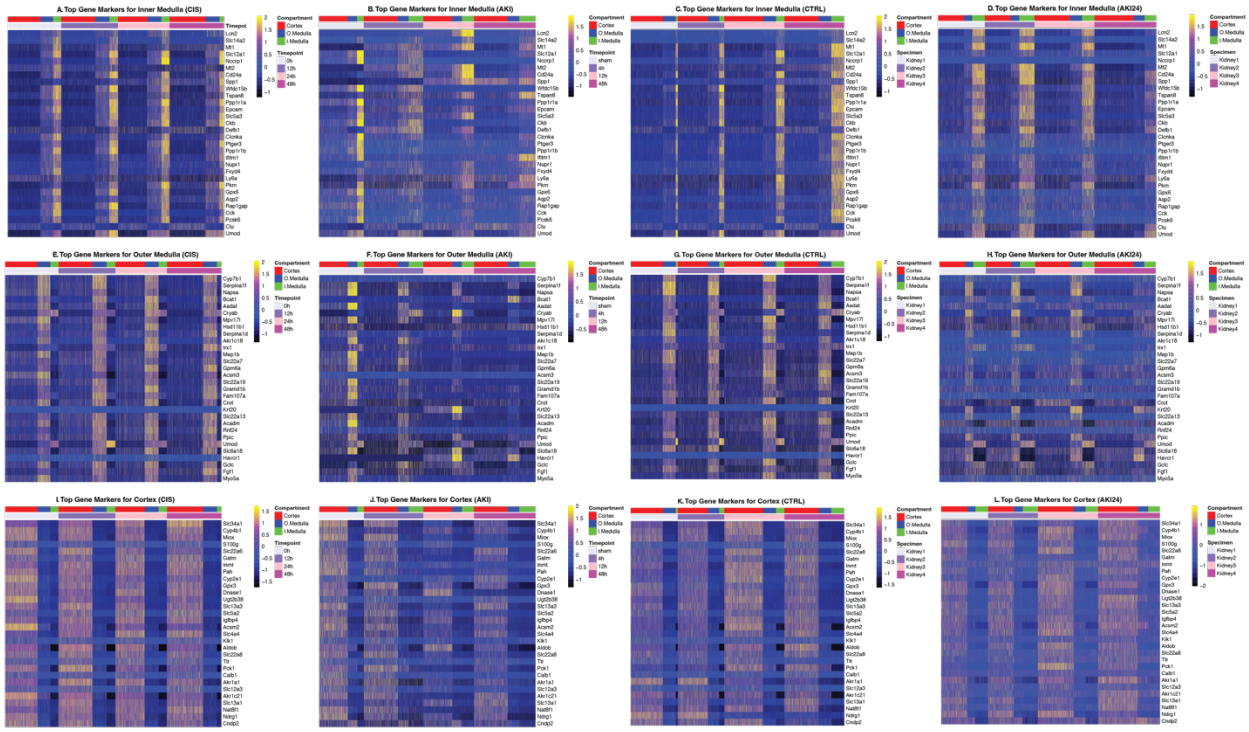

Figure S2. Heatmap of top compartment-specific marker genes for cold ischemia (CIS), warm ischemia-reperfusion-induced acute kidney injury (AKI), normal control kidneys (CTRL) and 24-hours warm ischemia-reperfusion-induced acute kidney injury (AKI24) injury datasets. Heatmap of top compartment-specific marker genes expression within the different kidney tissue compartments namely **(A,B,C,D)** inner medulla (I.medulla (green)), **(E,F,G,H)** outer medulla (O. medulla (blue)) and **(I,J,K,L)** cortex (red) belonging to different timepoints of cold ischemia (CIS) and ischemia-reperfusion (AKI) injury, normal control kidneys (CTRL) and 24-hours warm ischemic-reperfusion injury (AKI24) datasets respectively.

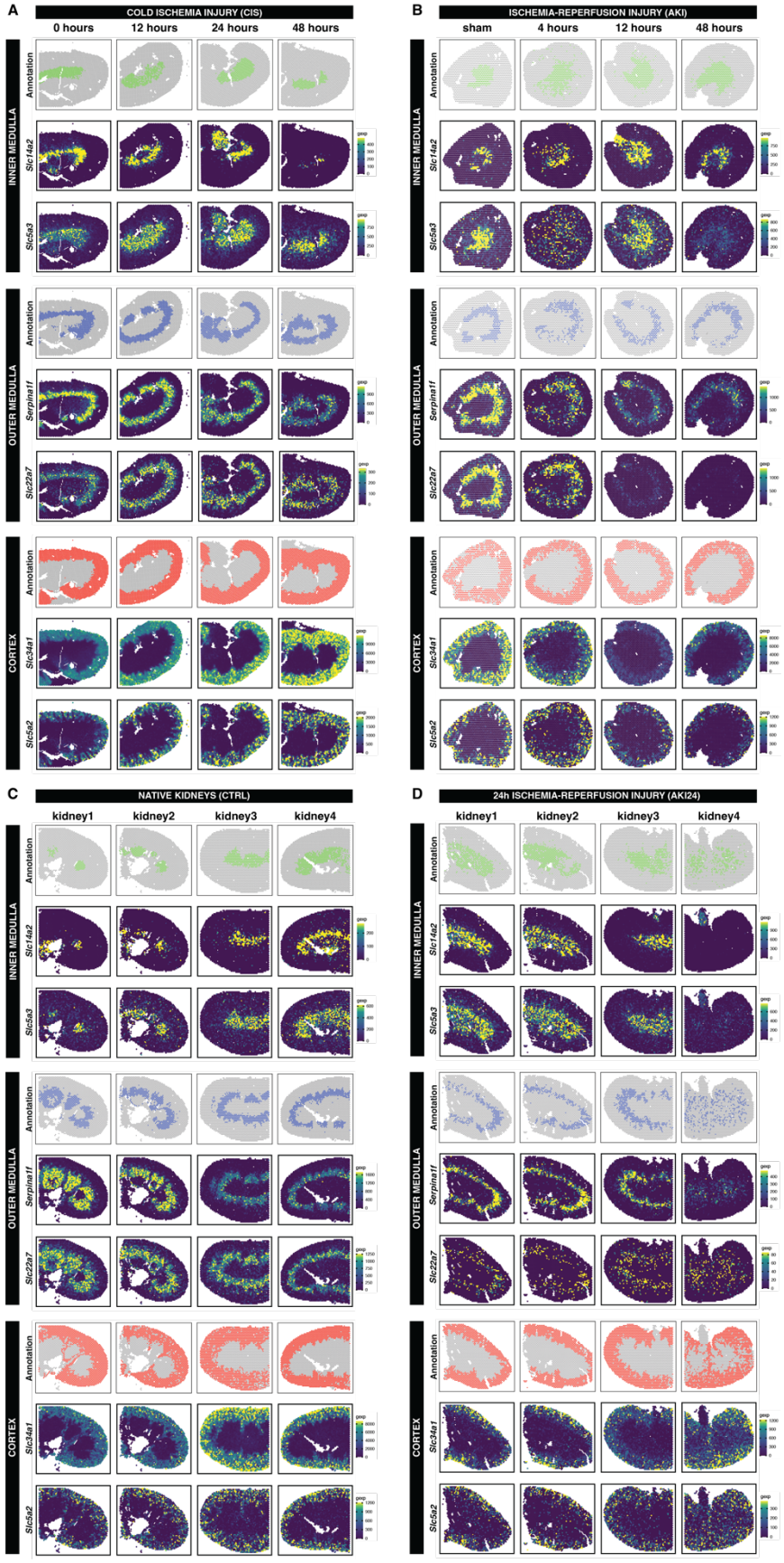
A
COLD ISCHEMIA INJURY (CIS)
0 hours
12 hours
24 hours
48 hours
B
ISCHEMIA-REPERFUSION INJURY (AKI)
sham
4 hours
12 hours
48 hours
C
NATIVE KIDNEYS (CTRL)
kidney1
kidney2
kidney3
kidney4
D
24h ISCHEMIA-REPERFUSION INJURY (AKI24)
kidney1
kidney2
kidney3
kidney4
INNER MEDULLA
OUTER MEDULLA
CORTEX
Annotation
Slc14a2
Slc5a3
Serpina1f
Slc22a7
Slc34a1
Slc5a2

Figure S3. Spatiotemporal expression patterns of compartment-specific marker genes in different experimental groups. Presentation of inner medulla marker genes (*Slc14a2*, *Slc5a3*); outer medulla marker genes (*Serpina1f, Slc22a7*); cortex marker genes (*Slc34a1, Slc5a2*) within the **(A)** cold ischemia injury (CIS), **(B)** warm ischemia-reperfusion injury (AKI), **(C)** normal control kidneys (CTRL) and **(D)** 24-hours warm ischemia-reperfusion injury (AKI24) kidney tissue specimens. Color coded annotations: red (cortex), blue (outer medulla), green (inner medulla) and other (gray), highlight the location of the different compartments within respective tissue specimens.

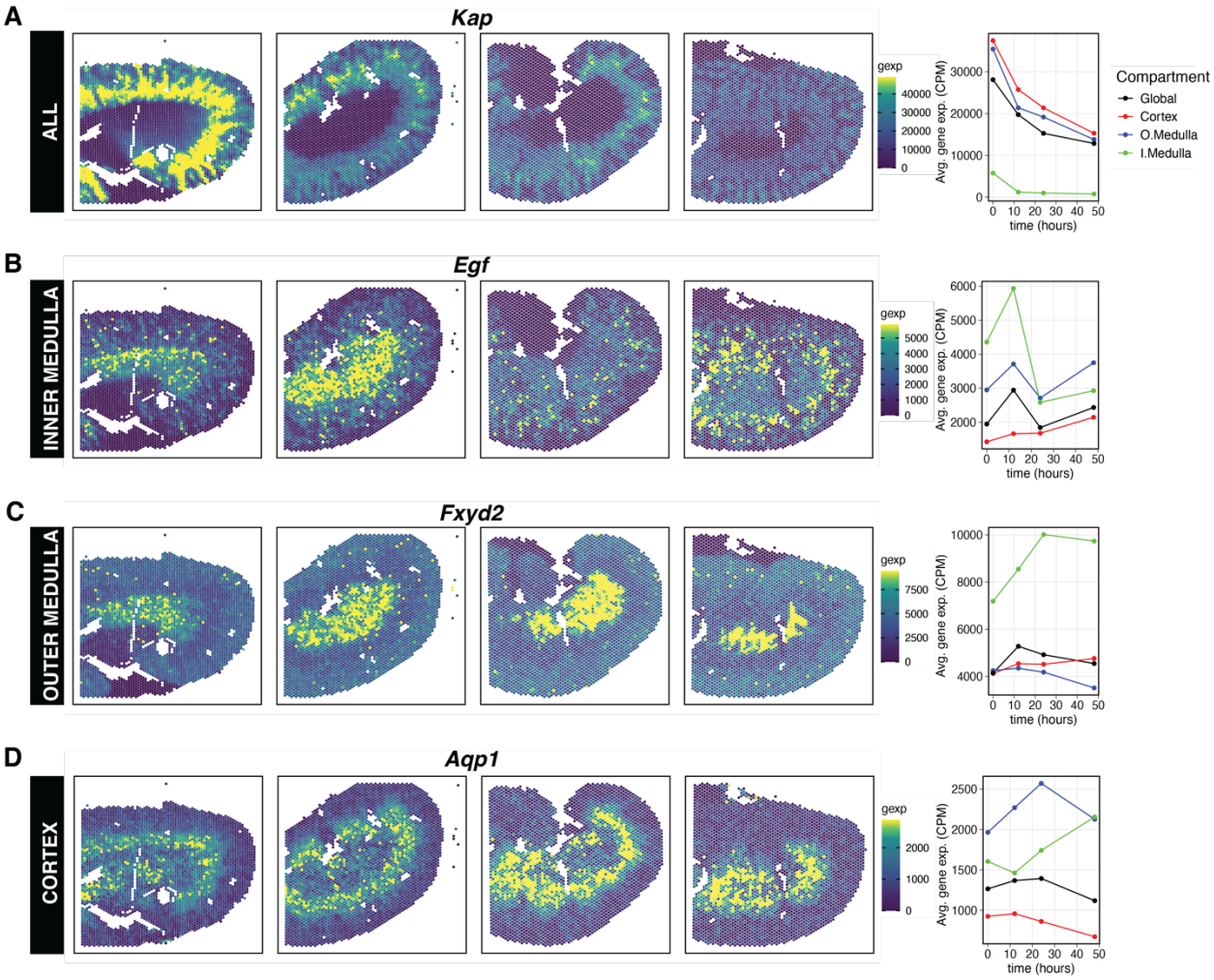

Figure S4. Representative genes demonstrating compartment-specific downward temporal trend in cold ischemic kidneys. While **(A)** *Kap* demonstrated temporally downward trend in all three compartments, **(B)** *Egf,* **(C)** *Fxyd2* and **(D)** *Aqp1* were confined to the inner medulla, outer medulla, and cortex respectively. The line plots demonstrate the mean expression (CPM normalized) of the respective genes within different compartments of the corresponding cold ischemic tissue at different time points.

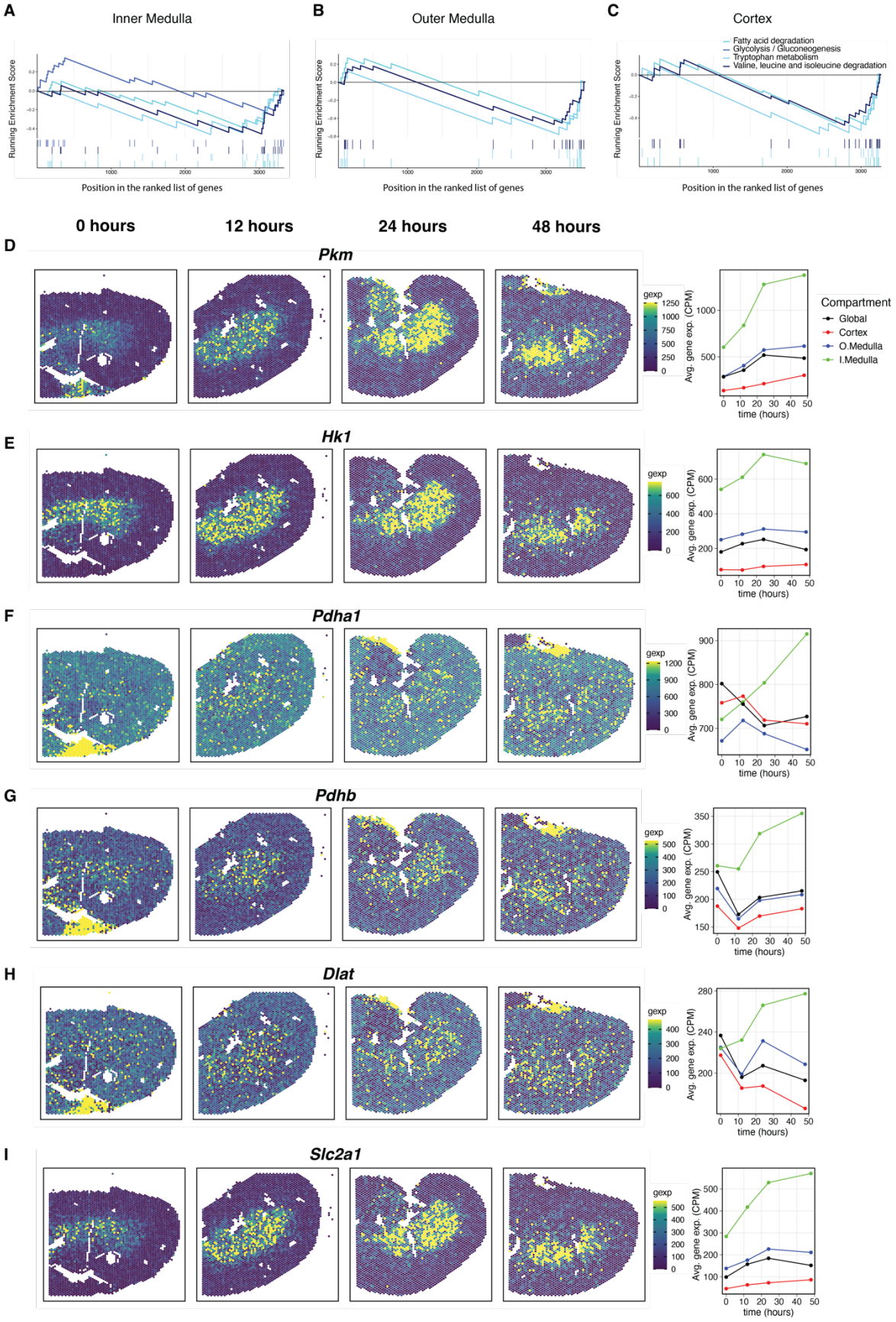
A
Inner Medulla
B
Outer Medulla
C
Cortex
Fatty acid degradation
Glycolysis / Gluconeogenesis
Tryptophan metabolism
Valine, leucine and isoleucine degradation
Running Enrichment Score
Position in the ranked list of genes
0 hours
12 hours
24 hours
48 hours
D
Pkm
E
Hk1
F
Pdha1
G
Pdhb
H
Dlat
I
Slc2a1
gexp
Avg. gene exp. (CPM)
time (hours)
Compartment
Global
Cortex
O.Medulla
I.Medulla

Figure S5. Compartment-specific enrichment of metabolic intermediate generating pathways in cold ischemic kidneys. Running enrichment score plots demonstrating differential enrichment of important metabolic intermediate generating pathways such as glycolysis/gluconeogenesis, fatty acid degradation, tryptophan metabolism, valine, leucine and isolecuine metabolism within the **(A)** inner medulla, **(B)** outer medulla and **(C)** cortex of cold ischemia injury kidneys. Spatial gene expression plots demonstrating spatiotemporal expression of genes related to metabolic processes like glycolysis **(D)** *Pkm,* **(E)** *Hk1;* coupling of glycolysis and TCA cycle like **(F)** *Pdha1,***(G)** *Pdhb,* **(H)** *Dlat* and glucose transport across the cell membrane like **(I)** *Slc2a1*. The line plots demonstrate the mean expression (CPM normalized) of the respective genes within different compartments of the corresponding cold ischemic tissue at different time points.

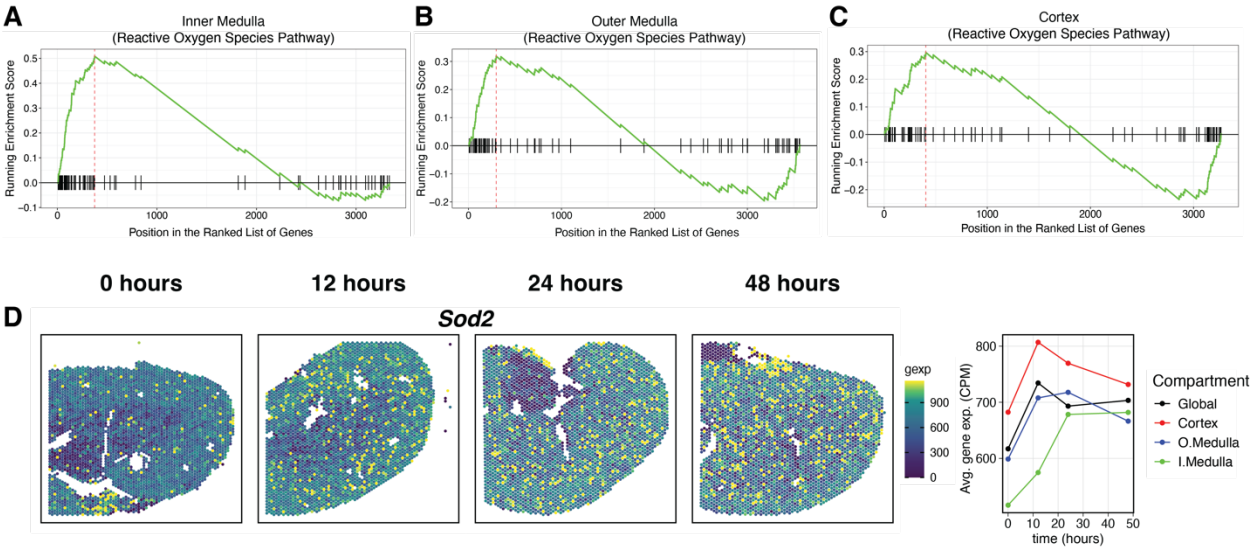

Figure S6. Enrichment of the reactive oxygen species pathway in different compartments of cold ischemic kidney tissue. Running enrichment score plots demonstrating enrichment of the reactive oxygen species pathway within the **(A)** inner medulla, **(B)** outer medulla and **(C)** cortex of cold ischemia injury kidneys. **(D)** Spatial gene expression plots and corresponding line plots demonstrating spatiotemporal dynamics of a gene in the reactive oxygen species pathway, *Sod2.*

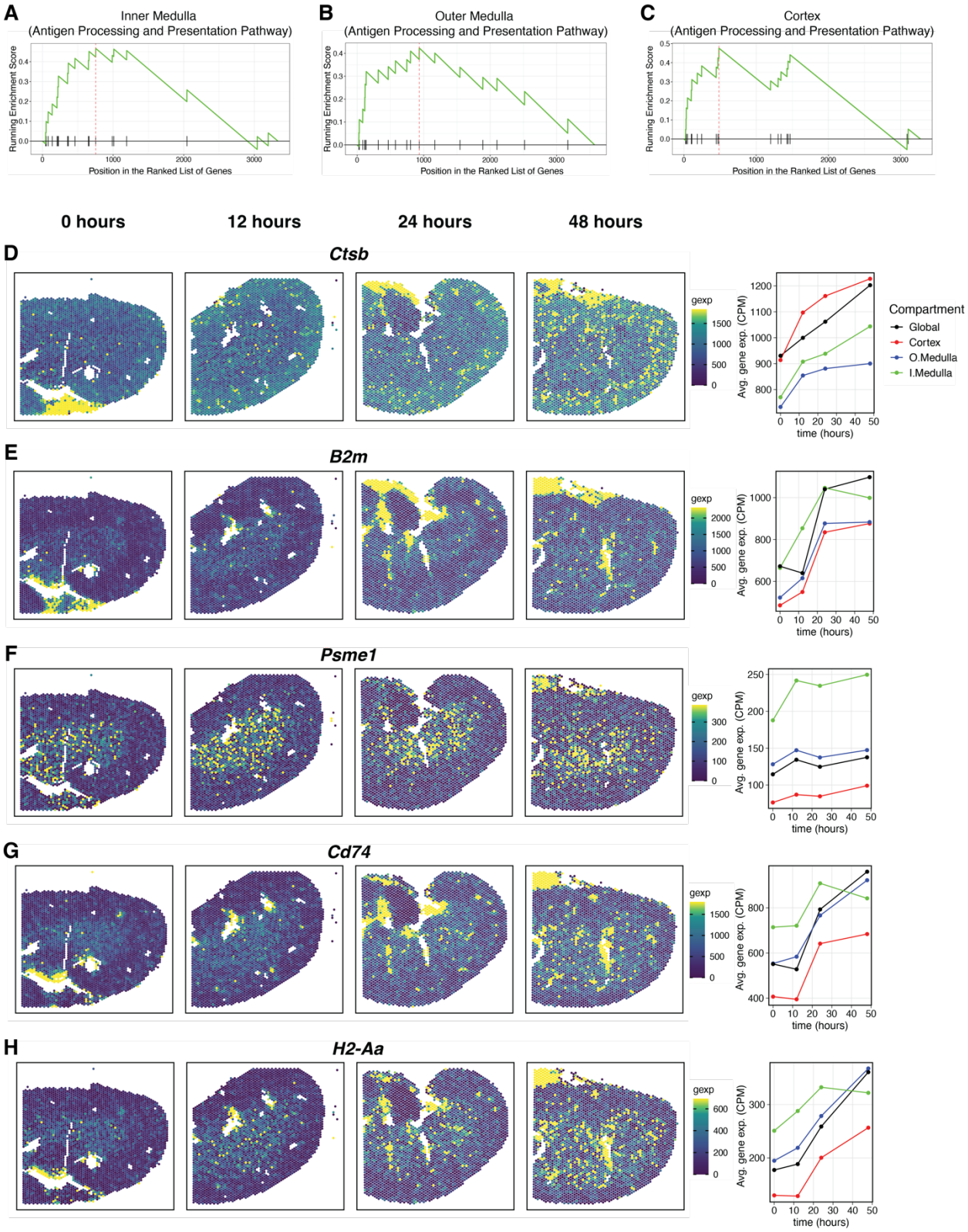
A
Inner Medulla
(Antigen Processing and Presentation Pathway)
B
Outer Medulla
(Antigen Processing and Presentation Pathway)
C
Cortex
(Antigen Processing and Presentation Pathway)
Running Enrichment Score
Position in the Ranked List of Genes
0 hours
12 hours
24 hours
48 hours
D
Ctsb
E
B2m
F
Psme1
G
Cd74
H
H2-Aa
gexp
Avg. gene exp. (CPM)
time (hours)
Compartment
Global
Cortex
O.Medulla
I.Medulla

Figure S7. Compartment-specific enrichment of antigen processing and presentation pathway in cold ischemic kidneys. Running enrichment score plots demonstrating enrichment of antigen processing and presentation pathway within the **(A)** inner medulla, **(B)** outer medulla and **(C)** cortex of cold ischemia injury kidneys. Spatial gene expression plots and corresponding line plots demonstrating spatiotemporal dynamics of genes within the antigen processing and presentation pathway: **(D)** *Ctsb,* **(E)** *B2m,* **(F)** *Psme1,* **(G)** *Cd74* and **(H)** *H2-Aa*.

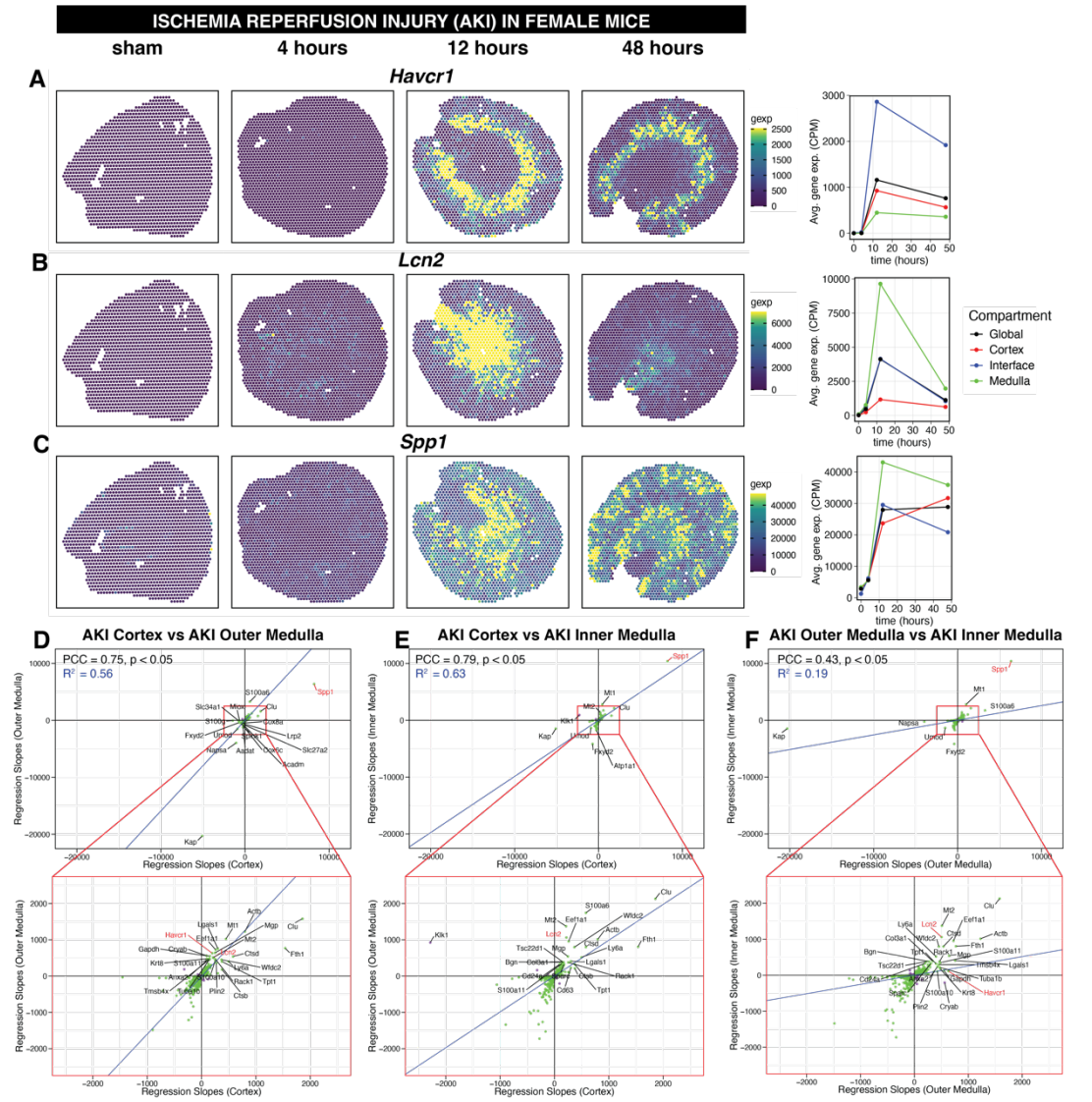
ISCHEMIA REPERFUSION INJURY (AKI) IN FEMALE MICE
sham
4 hours
12 hours
48 hours
A
Havcr1
B
Lcn2
C
Spp1
gexp
Avg. gene exp. (CPM)
time (hours)
Compartment
Global
Cortex
Interface
Medulla
D
AKI Cortex vs AKI Outer Medulla
PCC = 0.75, p < 0.05
R² = 0.56
E
AKI Cortex vs AKI Inner Medulla
PCC = 0.79, p < 0.05
R² = 0.63
F
AKI Outer Medulla vs AKI Inner Medulla
PCC = 0.43, p < 0.05
R² = 0.19
Regression Slopes (Outer Medulla)
Regression Slopes (Inner Medulla)
Regression Slopes (Cortex)

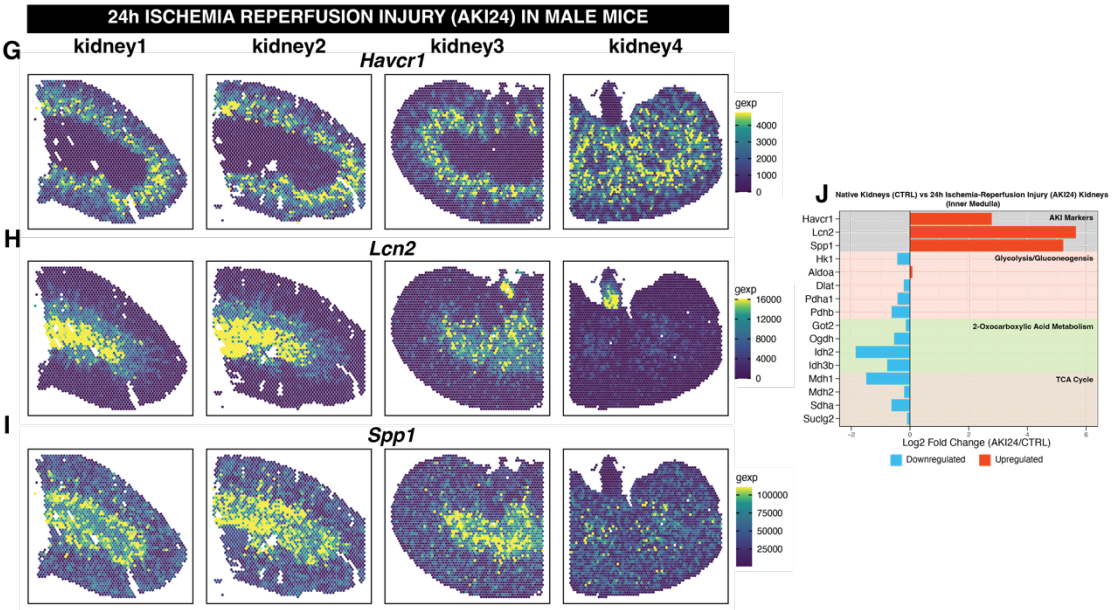
24h ISCHEMIA REPERFUSION INJURY (AKI24) IN MALE MICE
G
kidney1
kidney2
kidney3
kidney4
Havcr1
H
Lcn2
I
Spp1
gexp
J
Native Kidneys (CTRL) vs 24h Ischemia-Reperfusion Injury (AKI24) Kidneys (Inner Medulla)
AKI Markers
Glycolysis/Gluconeogenesis
2-Oxocarboxylic Acid Metabolism
TCA Cycle
Log2 Fold Change (AKI24/CTRL)
Downregulated
Upregulated

Figure S8. Spatiotemporal transcriptional dynamics within female and male experimental models of warm ischemia-reperfusion injury (i.e., AKI and AKI24). Spatial plots depicting the spatiotemporal expression of putative AKI marker genes like **(A)** *Havcr1,* **(B)** *Lcn2* and **(C)** *Spp1* within warm ischemia-reperfusion injury (AKI) kidney tissue specimens from female murine models. Scatter plots depicting the correlation analysis of the temporal transcriptional dynamics between the different compartments: **(D)** cortex vs outer medulla **(E)** cortex vs inner medulla and **(F)** outer medulla vs inner medulla of the acute kidney injury (AKI) tissue. Genes exhibiting covarying (green) or divergent (purple) temporal trend within these compartments can be visualized along with their Pearson correlation coefficients (PCC) and linear regression slopes (blue line). AKI marker genes like *Spp1, Havcr1 and Lcn2* within these compartments have been highlighted red. Spatial plots depicting the spatiotemporal expression of **(G)** *Havcr1,* **(H)** *Lcn2* and **(I)** *Spp1* within 24-hours warm ischemia-reperfusion injury (AKI24) kidney tissue specimens from male murine models. **(J)** Barplots highlighting differential expression fold change of AKI marker genes (*Havcr1, Lcn2, Spp1*) and genes related to pathways like glycolysis/gluconeogenesis (*Hk1, Aldoa, Dlat, Pdha1, Pdhb*), 2-oxycarboxylic acid metabolism (*Got2, Ogdh, Idh2, Idh3b*) and TCA cycle (*Mdh1, Mdh2, Sdha, Suclg2*) between the 24-hours warm ischemia-reperfusion injury (AKI24) versus normal control kidneys (CTRL) kidney tissue specimens.

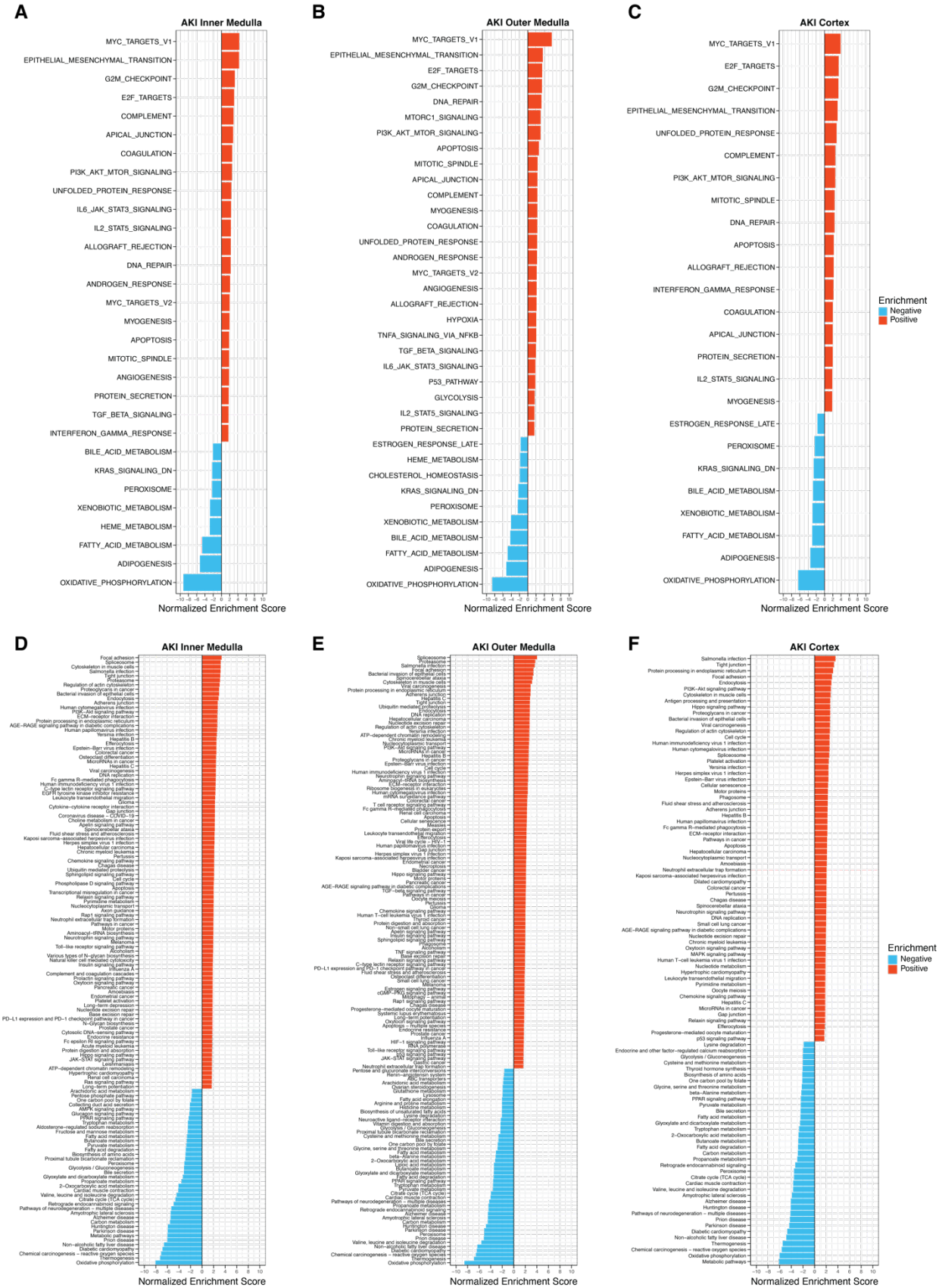
A
AKI Inner Medulla
MYC_TARGETS_V1
EPITHELIAL_MESENCHYMAL_TRANSITION
G2M_CHECKPOINT
E2F_TARGETS
COMPLEMENT
APICAL_JUNCTION
COAGULATION
PI3K_AKT_MTOR_SIGNALING
UNFOLDED_PROTEIN_RESPONSE
IL6_JAK_STAT3_SIGNALING
IL2_STAT5_SIGNALING
ALLOGRAFT_REJECTION
DNA_REPAIR
ANDROGEN_RESPONSE
MYC_TARGETS_V2
MYOGENESIS
APOPTOSIS
MITOTIC_SPINDLE
ANGIOGENESIS
PROTEIN_SECRETION
TGF_BETA_SIGNALING
INTERFERON_GAMMA_RESPONSE
BILE_ACID_METABOLISM
KRAS_SIGNALING_DN
PEROXISOME
XENOBIOTIC_METABOLISM
HEME_METABOLISM
FATTY_ACID_METABOLISM
ADIPOGENESIS
OXIDATIVE_PHOSPHORYLATION
Normalized Enrichment Score
B
AKI Outer Medulla
MYC_TARGETS_V1
EPITHELIAL_MESENCHYMAL_TRANSITION
E2F_TARGETS
G2M_CHECKPOINT
DNA_REPAIR
MTORC1_SIGNALING
PI3K_AKT_MTOR_SIGNALING
APOPTOSIS
MITOTIC_SPINDLE
APICAL_JUNCTION
COMPLEMENT
MYOGENESIS
COAGULATION
UNFOLDED_PROTEIN_RESPONSE
ANDROGEN_RESPONSE
MYC_TARGETS_V2
ANGIOGENESIS
ALLOGRAFT_REJECTION
HYPOXIA
TNFA_SIGNALING_VIA_NFKB
TGF_BETA_SIGNALING
IL6_JAK_STAT3_SIGNALING
P53_PATHWAY
GLYCOLYSIS
IL2_STAT5_SIGNALING
PROTEIN_SECRETION
ESTROGEN_RESPONSE_LATE
HEME_METABOLISM
CHOLESTEROL_HOMEOSTASIS
KRAS_SIGNALING_DN
PEROXISOME
XENOBIOTIC_METABOLISM
BILE_ACID_METABOLISM
FATTY_ACID_METABOLISM
ADIPOGENESIS
OXIDATIVE_PHOSPHORYLATION
Normalized Enrichment Score
C
AKI Cortex
MYC_TARGETS_V1
E2F_TARGETS
G2M_CHECKPOINT
EPITHELIAL_MESENCHYMAL_TRANSITION
UNFOLDED_PROTEIN_RESPONSE
COMPLEMENT
PI3K_AKT_MTOR_SIGNALING
MITOTIC_SPINDLE
DNA_REPAIR
APOPTOSIS
ALLOGRAFT_REJECTION
INTERFERON_GAMMA_RESPONSE
COAGULATION
APICAL_JUNCTION
PROTEIN_SECRETION
IL2_STAT5_SIGNALING
MYOGENESIS
ESTROGEN_RESPONSE_LATE
PEROXISOME
KRAS_SIGNALING_DN
BILE_ACID_METABOLISM
XENOBIOTIC_METABOLISM
FATTY_ACID_METABOLISM
ADIPOGENESIS
OXIDATIVE_PHOSPHORYLATION
Normalized Enrichment Score
Enrichment
Negative
Positive
D
AKI Inner Medulla
Normalized Enrichment Score
E
AKI Outer Medulla
Normalized Enrichment Score
F
AKI Cortex
Normalized Enrichment Score
Enrichment
Negative
Positive

Figure S9. Compartment-specific enrichment of molecular pathways within acute kidney injury (AKI) tissues. Bar plots highlighting all the enriched molecular pathways (Hallmark) that demonstrated similar temporal dynamics (enrichment: positive (red), negative (cyan)) within the corresponding **(A)** inner medulla, **(B)** outer medulla and **(C)** cortex of warm ischemia-reperfusion injury (AKI) renal tissue. Similar, bar plots highlighting all the enriched molecular pathways (KEGG) that demonstrated similar temporal dynamics (enrichment: positive (red), negative (cyan)) within the corresponding **(D)** inner medulla, **(E)** outer medulla and **(F)** cortex of warm ischemia-reperfusion injury (AKI) renal tissue.

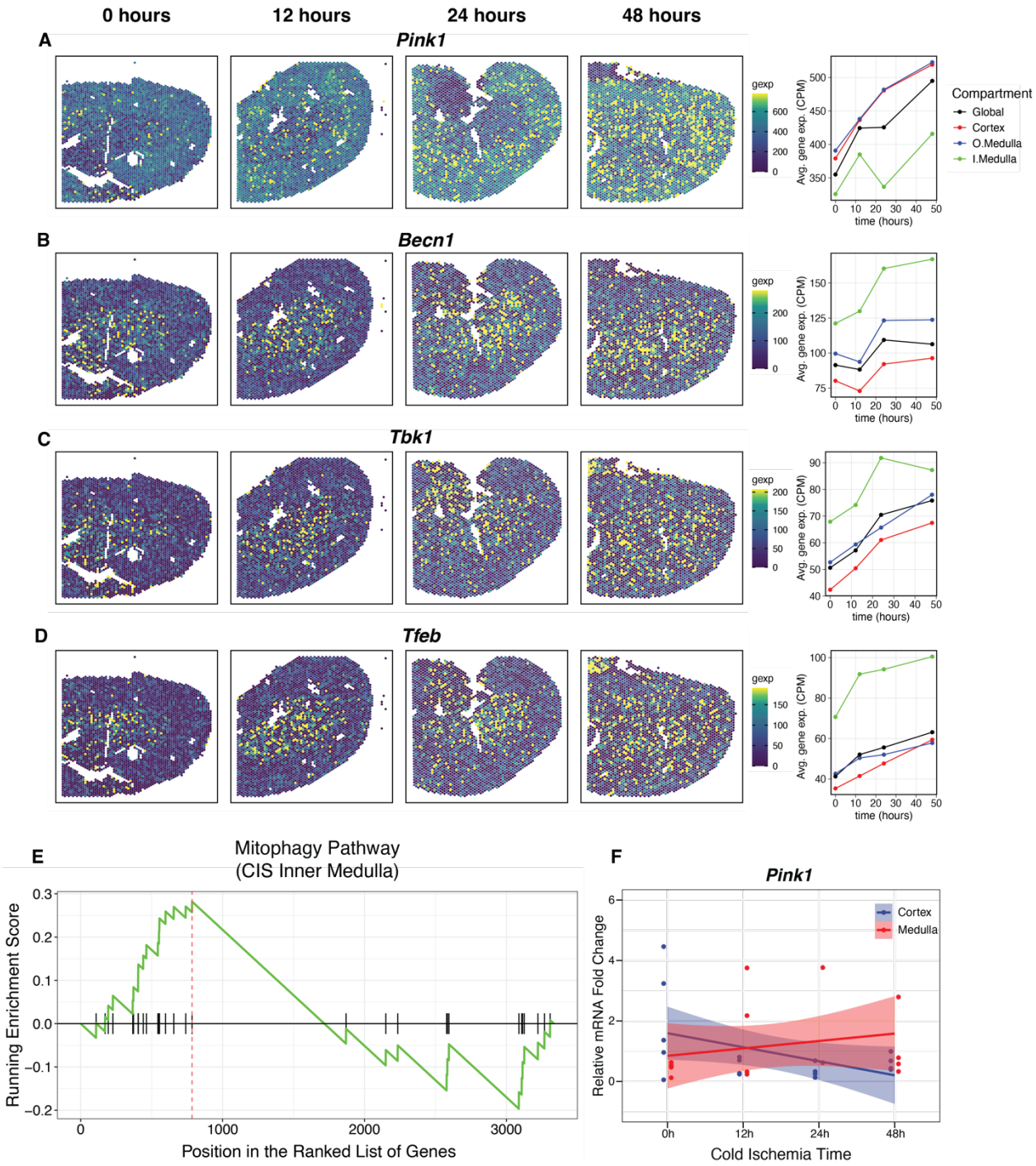

Figure S10. Mitophagy pathway progression within cold ischemia kidney tissue. Spatial gene plots demonstrating spatiotemporal expression of mitophagy related genes **(A)** *Pink1*, **(B)** *Becn1*, **(C)** *Tbk1,* and **(D)** *Tfeb* within the cold ischemia kidney tissue. **(E)** Running enrichment score plot of mitophagy pathway

within the inner medulla of cold ischemia tissue. **(F)** Quantitative qPCR comparison of *Pink1* between the cortex and medulla (inner medulla + outer medulla) compartments of renal tissue at different time points of cold ischemia injury.

Supplementary Table Legends

Supplementary Table 1. Temporally downregulated genes. List of genes that demonstrated a downward temporal trend during cold ischemia injury with the inner medulla (sheet 1), outer medulla (sheet 2) and cortex (sheet 3) of the renal tissue. Genes are ordered according to their linear regression slopes with the gene demonstrating the maximum temporal change at the top and the minimum at the bottom.

Supplementary Table 2. Temporally upregulated genes. List of genes that demonstrated an upward temporal trend during cold ischemia injury with the inner medulla (sheet 1), outer medulla (sheet 2) and cortex (sheet 3) of the renal tissue. Genes are ordered according to their linear regression slopes with the gene demonstrating the maximum temporal change at the top and the minimum at the bottom.

Supplementary Table 3. Temporally regulated genes shared across all kidney compartments. List of genes that demonstrated a downward (sheet 1) or upward (sheet 2) temporal trend during cold ischemia injury shared across all compartments of the renal tissue.

Supplementary Table 4. Temporally upregulated genes unique to a particular kidney compartment. List of genes that demonstrated an upward temporal trend during cold ischemia injury that was compartmentally confined to the inner medulla (sheet 1), outer medulla (sheet 2) and cortex (sheet 3) of the renal tissue. Genes are ordered according to their linear regression slopes with the gene demonstrating the maximum temporal change at the top and the minimum at the bottom.

Supplementary Table 5. Temporally downregulated genes unique to a particular kidney compartment. List of genes that demonstrated a downward temporal trend during cold ischemia injury that was compartmentally confined to the inner medulla (sheet 1), outer medulla (sheet 2) and cortex (sheet 3) of the renal tissue. Genes are ordered according to their linear regression slopes with the gene demonstrating the maximum temporal change at the top and the minimum at the bottom.

Supplementary Table 6. Enriched molecular (KEGG) pathways within different compartments of kidney during cold ischemia (CIS) injury. List of enriched molecular pathways (KEGG) associated with genes that demonstrated a significant temporal trend (either upward or downward) during cold ischemia injury within the inner medulla (sheet 1), outer medulla (sheet 2) and cortex (sheet 3) of the CIS renal tissue. Molecular pathways are ordered according to their normalized enrichment scores (NES) obtained from gene set enrichment analysis with pathways with highest NES at the top and minimum NES at the bottom. Corresponding adjusted p-values (p.adjust) and genes with significant contribution to the NES (Leading Edge Genes) for the respective enriched pathways are also provided. Pathways with p.adjust<0.05 are not included in the list.

Supplementary Table 7. Enriched molecular (Hallmark gene sets of MSigDB) pathways within different compartments of kidney during cold ischemia (CIS) injury. List of enriched molecular pathways (Hallmark gene sets of MSigDB) associated with genes that demonstrated a significant temporal trend (either upward or downward) during cold ischemia injury within the inner medulla (sheet 1), outer medulla (sheet 2) and cortex (sheet 3) of the CIS renal tissue. Molecular pathways are ordered according to their normalized enrichment scores (NES) obtained from gene set enrichment analysis with pathways with highest NES at the top and minimum NES at the bottom. Corresponding adjusted p-values (p.adjust) and genes with significant contribution to the NES (Leading Edge Genes) for the respective enriched pathways are also provided. Pathways with p.adjust<0.05 are not included in the list.

Supplementary Table 8. Enriched molecular (KEGG) pathways within different compartments of kidney during warm ischemia-reperfusion (AKI) injury. List of enriched molecular pathways (KEGG) associated with genes that demonstrated a significant temporal trend (either upward or downward) during warm ischemia-reperfusion injury within the inner medulla (sheet 1), outer medulla (sheet 2) and cortex (sheet 3) of the AKI renal tissue. Molecular pathways are ordered according to their normalized enrichment scores (NES) obtained from gene set enrichment analysis with pathways with highest NES at the top and minimum NES at the bottom. Corresponding adjusted p-values (p.adjust) and genes with significant contribution to the NES (Leading Edge Genes) for the respective enriched pathways are also provided. Pathways with p.adjust<0.05 are not included in the list.

Supplementary Table 9. Enriched molecular (Hallmark gene sets of MSigDB) pathways within different compartments of kidney during warm ischemia-reperfusion (AKI) injury. List of enriched molecular pathways (Hallmark gene sets of MSigDB) associated with genes that demonstrated a significant temporal trend (either upward or downward) during warm ischemia-reperfusion injury within the inner medulla (sheet 1), outer medulla (sheet 2) and cortex (sheet 3) of the AKI renal tissue. Molecular pathways are ordered according to their normalized enrichment scores (NES) obtained from gene set enrichment analysis with pathways with highest NES at the top and minimum NES at the bottom. Corresponding adjusted p-values (p.adjust) and genes with significant contribution to the NES (Leading Edge Genes) for the respective enriched pathways are also provided. Pathways with p.adjust<0.05 are not included in the list.